WRDC-TR-90-4001

AD-A220 239

FATIGUE CRACK GROWTH INVESTIGATION OF A Ti-6Al-4V FORGING UNDER COMPLEX LOADING CONDITIONS - NATO/AGARD SUPPLEMENTAL ENGINE DISK PROGRAM

John J. Ruschau
UNIVERSITY OF DAYTON RESEARCH INSTITUTE
300 COLLEGE PARK AVENUE
DAYTON, OHIO 45469

Peter A. Krawczyk, 1Lt, USAF
MATERIALS ENGINEERING BRANCH
SYSTEMS SUPPORT DIVISION
WRIGHT-PATTERSON AFB, OHIO 45433

February 1990

Interim Report for Period June 1988 - October 1989

MATERIALS LABORATORY
WRIGHT RESEARCH AND DEVELOPMENT CENTER
AIR FORCE SYSTEMS COMMAND
WRIGHT-PATTERSON AIR FORCE BASE, OH 45433-6533

NOTICE

WHEN GOVERNMENT DRAWINGS, SPECIFICATIONS, OR OTHER DATA ARE USED FOR ANY PURPOSE OTHER THAN IN CONNECTION WITH A DEFINITELY GOVERNMENT-RELATED PROCUREMENT, THE UNITED STATES GOVERNMENT INCURS NO RESPONSIBILITY OR ANY OBLIGATION WHATSOEVER. THE FACT THAT THE GOVERNMENT MAY HAVE FORMULATED OR IN ANY WAY SUPPLIED THE SAID DRAWINGS, SPECIFICATIONS, OR OTHER DATA, IS NOT TO BE REGARDED BY IMPLICATION, OR OTHERWISE IN any MANNER CONSTRUED, AS LICENSING THE HOLDER, OR ANY OTHER PERSON OR CORPORATION; OR AS CONVEYING ANY RIGHTS OR PERMISSION TO MANUFACTURE, USE, OR SELL ANY PATENTED INVENTION THAT MAY IN ANY WAY BE RELATED THERETO.

THIS REPORT HAS BEEN REVIEWED BY THE OFFICE OF PUBLIC AFFAIRS (ASD/PA) AND IS RELEASABLE TO THE NATIONAL TECHNICAL INFORMATION SERVICE (NTIS). AT NTIS IT WILL BE AVAILABLE TO THE GENERAL PUBLIC INCLUDING FOREIGN NATIONS.

THIS TECHNICAL REPORT HAS BEEN REVIEWED AND IS APPROVED FOR PUBLICATION.

Peter A. Krawczyk

LT. PETER A. KRAWCZYK
Engineering and Design Data
Materials Engineering Branch

Clayton L. Harmsworth

CLAYTON L. HARMSWORTH
Technical Manager
Engineering and Design Data
Materials Engineering Branch

FOR THE COMMANDER

T.J. Reinhart

T.J. REINHART, Chief
Materials Engineering Branch
Materials Laboratory

IF YOUR ADDRESS HAS CHANGED, IF YOU WISH TO BE REMOVED FROM OUR MAILING LIST, OR IF THE ADDRESSEE IS NO LONGER EMPLOYED BY YOUR ORGANIZATION PLEASE NOTIFY WRDC/MLSE , WRIGHT-PATTERSON AFB, OH 45433-6533 TO HELP MAINTAIN A CURRENT MAILING LIST.

COPIES OF THIS REPORT SHOULD NOT BE RETURNED UNLESS RETURN IS REQUIRED BY SECURITY CONSIDERATIONS, CONTRACTUAL OBLIGATIONS, OR NOTICE ON A SPECIFIC DOCUMENT.

REPORT DOCUMENTATION PAGE

Form Approved OMB No. 0704-0188

1a. REPORT SECURITY CLASSIFICATION: Unclassified	1b. RESTRICTIVE MARKINGS
2a. SECURITY CLASSIFICATION AUTHORITY	3. DISTRIBUTION/AVAILABILITY OF REPORT: Approved for public release; distribution unlimited.
2b. DECLASSIFICATION/DOWNGRADING SCHEDULE	
4. PERFORMING ORGANIZATION REPORT NUMBER(S): UDR-TR-89-114	5. MONITORING ORGANIZATION REPORT NUMBER(S): WRDC-TR-90-4001
6a. NAME OF PERFORMING ORGANIZATION: University of Dayton Research Institute; 6b. OFFICE SYMBOL (If applicable)	7a. NAME OF MONITORING ORGANIZATION: Wright Research and Development Center Materials Laboratory (WRDC/MLSE)
6c. ADDRESS (City, State, and ZIP Code): 300 College Park Avenue Dayton, OH 45469	7b. ADDRESS (City, State, and ZIP Code): Wright-Patterson AFB, OH 45433-6533
8a. NAME OF FUNDING/SPONSORING ORGANIZATION; 8b. OFFICE SYMBOL (If applicable)	9. PROCUREMENT INSTRUMENT IDENTIFICATION NUMBER: F33615-88-C-5437
8c. ADDRESS (City, State, and ZIP Code)	10. SOURCE OF FUNDING NUMBERS

PROGRAM ELEMENT NO.	PROJECT NO.	TASK NO	WORK UNIT ACCESSION NO.
62102F	2418	07	03

11. TITLE (Include Security Classification) FATIGUE CRACK GROWTH INVESTIGATION OF A Ti-6Al-4V FORGING UNDER COMPLEX LOADING CONDITIONS - NATO/AGARD SUPPLEMENTAL ENGINE DISK PROGRAM

12. PERSONAL AUTHOR(S): John J. Ruschau and Peter A. Krawczyk, 1LT, USAF

13a. TYPE OF REPORT	13b. TIME COVERED	14. DATE OF REPORT (Year, Month, Day)	15. PAGE COUNT
Interim	FROM 6/88 TO 10/89	February 1990	73

16. SUPPLEMENTARY NOTATION

17. COSATI CODES			18. SUBJECT TERMS (Continue on reverse if necessary and identify by block number)
FIELD	GROUP	SUB-GROUP	Fatigue crack growth; TURBISTAN; Ti-6-4; NATO/AGARD/SMP; Striation
11	04		

19. ABSTRACT (Continue on reverse if necessary and identify by block number)

Fatigue crack growth rate testing was performed on a Ti-6Al-4V engine disk forging as part of the SUPPLEMENTAL Engine Disk Program sponsored by the North Atlantic Treaty Organization's Advisory Group for Aerospace Research and Development (NATO/AGARD). Such data were developed under room temperature conditions under a variety of load histories, ranging from constant amplitude with periodic overload to various forms of the TURBISTAN engine spectrum. The effects of each loading condition are examined with respect to fatigue crack growth rates. Crack growth mechanisms are identified for the various load histories based on SEM examinations. Comparisons are made between crack growth rates determined via electric potential methodology and those from fatigue striation measurements.

20. DISTRIBUTION/AVAILABILITY OF ABSTRACT: ☒ UNCLASSIFIED/UNLIMITED ☐ SAME AS RPT. ☐ DTIC USERS	21. ABSTRACT SECURITY CLASSIFICATION: Unclassified
22a NAME OF RESPONSIBLE INDIVIDUAL: C.L. Harmsworth	22b. TELEPHONE (Include Area Code): 513-255-5063; 22c. OFFICE SYMBOL: WRDC/MLSE

DD Form 1473, JUN 86 *Previous editions are obsolete.*

PREFACE

This technical report represents work conducted in support of the Structures and Material Panel (SMP) of the North American Treaty Organization, Advisory Group for Aerospace Research and Development (NATO/AGARD). Work was performed by the Materials Branch (WRDC/MLSE) of the Systems Support Division, Materials Laboratory, Wright Research and Development Center, WPAFB, Ohio, and supported by the University of Dayton Research Institute, Dayton, Ohio, under Contract F33615-88-C-5437, "Quick Reaction Evaluation of Materials," with Mr. Neal Ontko serving as contract monitor.

This effort was conducted during the period of June 1988 to October 1989. The authors, Mr. John J. Ruschau and Lt. Peter A. Krawczyk, would like to extend special recognition to Mr. John H. Eblin of the University of Dayton who performed all mechanical testing, and to Dr. Kumar V. Jata, also of the University of Dayton, for his assistance in the fractographic investigations and technical review of this document.

This report was submitted by the authors in November 1989.

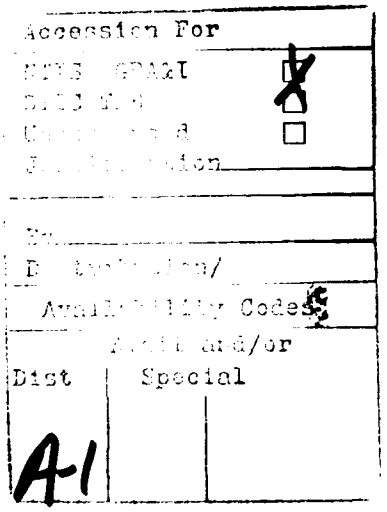

TABLE OF CONTENTS

LIST OF FIGURES

LIST OF FIGURES (Concluded)

SECTION 1
INTRODUCTION

Since 1970, the USAF has applied a damage tolerance design philosophy in the design of aircraft structures; however, the application of such fracture mechanics methodology to aircraft engine components, specifically for life prediction of engine disks, is a recent development. Although MIL-STD-1783, which deals with damage tolerance requirements for aircraft engines has been established, engine disk design is currently based on the safe-life design philosophy.

Interest by the North Atlantic Treaty Organization's Advisory Group for Aerospace Research and Development, NATO/AGARD, in applying damage tolerant concepts to engine disk design and life prediction resulted in an international test program to determine the fatigue crack growth and fracture behavior of engine disk materials under operational loading conditions. Twelve laboratories located throughout Europe and North America are actively involved in this effort, with Wright Research and Development Center's Materials Laboratory (WRDC/MLSE) being one of three USA participants.

This effort was divided into a CORE program and a SUPPLEMENTAL program. The CORE program, completed in 1987, accomplished three things: it familiarized the participating laboratories with automated data acquisition techniques, specifically the electric potential difference (EPD) technique for crack length measurement; it standardized test specimens and test techniques; and it generated fatigue crack growth rate data on Ti-6-4 to verify current life prediction models.[1-3] The purpose of the SUPPLEMENTAL program, described herein, was to generate low cycle fatigue and fatigue crack growth rate data on three engine disk alloys, Ti-6-4, IMI 685, and Ti-17, under variable loading conditions. Data generated in this program will then be used to assist in life prediction models. The role of this laboratory in this SUPPLEMENTAL effort was to generate fatigue crack growth rate data on the Ti-6-4 material under both simple and complex loading histories.

SECTION 2
MATERIALS AND SPECIMENS

2.1 MATERIALS

The material examined in this program was a Ti-6Al-4V disk forging which was furnished by the test organizers in the solution-heat-treated and aged (STA) condition. The microstructure of this material, shown in Figure 1, consists of equiaxed alpha grains in a transformed beta matrix containing coarse, acicular alpha. The microstructure is almost identical to that reported in the CORE program results [1] except that occasional alignment of the alpha grains is not observed. Metallographic examinations for the radial, tangential, and thickness directions showed no significant microstructural differences, indicating a fairly homogeneous structure. A chemical analysis was performed on one failed specimen (CP26) to determine chemical composition. Results of this analysis are shown in Table 1. The amounts indicated in the table are all within the limits as specified in MIL-T-9047, "Aircraft Quality Titanium and Titanium Alloy Bars and Reforging Stock".

2.2 SPECIMEN DESIGN

Sixteen standard C(T) specimens were machined from this material and supplied by Rolls Royce LTD, designated CP21 through CP30 and CP37 through CP42. Threaded holes for attaching the electric potential current wires were machined in the supplied samples, located along the load-line of each sample. Nominal specimen dimensions are shown in Figure 2.

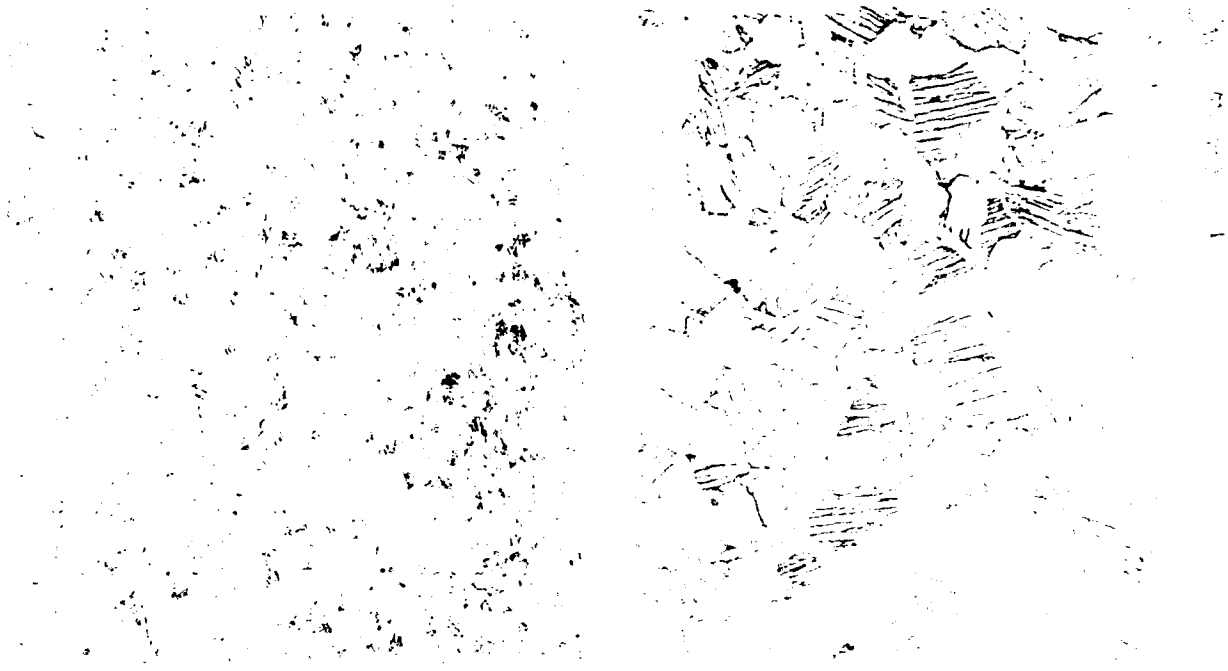

Figure 1. Microstructure of Ti-6Al-4V disk forging at (a) 100X and (b) 500X.

TABLE 1

CHEMICAL COMPOSITION OF Ti-6Al-4V DISK FORGING

Ti-6-4	Element	Al	V	Fe	Ti
CP26	w/o	6.11	4.08	0.23	Rem
MIL-T-9047G	w/o	5.50 - 6.75	3.5 - 4.5	0.3 max	---

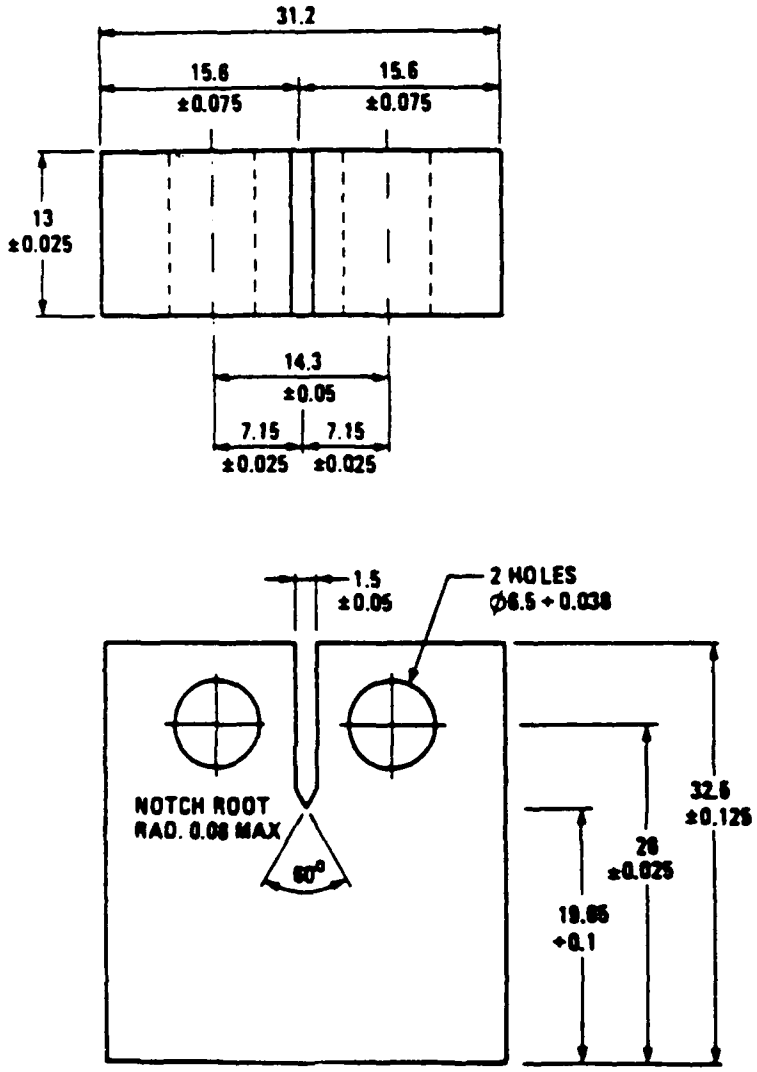

Figure 2. C(T) specimen for Ti-6Al-4V disk forging.

SECTION 3
TEST PROCEDURES

All testing was performed in an MTS servo-hydraulic test machine under lab air conditions. An HP Model 216 computer system, equipped with an HP 6942 Multiprogrammer, was used to apply the various load histories and check feedback to insure proper loading conditions. General procedures describing the required loading waveforms and methods for crack length determination were furnished by the test coordinators [4] and described briefly in the following paragraphs.

Two categories of load sequences were investigated: simplified and complex. The four simplified sequences, identified as Types 1 through 4, are illustrated in Figure 3. Types 1, 2, and 3 are similar with respect to waveshape, with differences only in the magnitude of the ten, low amplitude "subcycles" which occur at the peak of the major load cycle. The amplitude of the subcycles was 10 percent of the maximum load for the Type 1 sequence, 30 percent for Type 2, and 50 percent for Type 3. Loading rate for all three of these sequences was identical at zero-maximum in 1 second, with minimum load at slightly above zero to avoid any backlash in the gripping assembly.

The Type 4 sequence is unique to Types 1 through 3 and represents 1000 constant amplitude (CA) load cycles at an R-ratio of 0.1, followed by a single overload cycle at 1.7 of the CA maximum load. Loading rates were faster than those for Types 1 through 3, with loading frequency at approximately 5 Hz.

The four complex load histories examined were the basic Cold TURBISTAN [5] load history, along with three variations of TURBISTAN in which several low amplitude loads were omitted, i.e., 10, 30, and 50 percent omission levels. A portion of each complex load history is furnished in Figure 4.

For all tests, crack length measurements were obtained using electric potential difference (EPD) technique developed during the CORE program, and verified with periodic visual surface measurements throughout each test. Electric potential measurements were

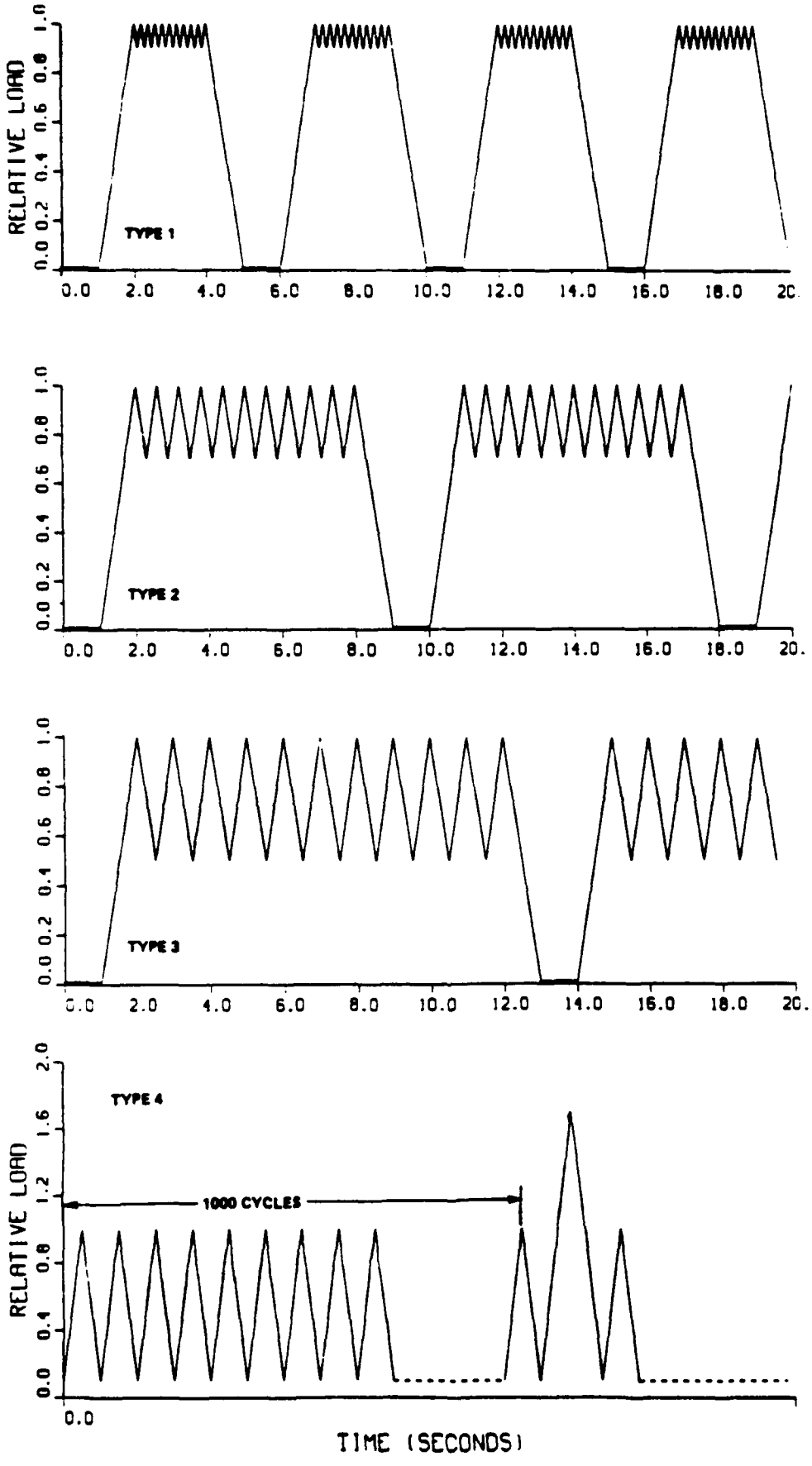

Figure 3. Simplified load sequences used in the NATO/AGARD SUPPLEMENTAL engine disk program.

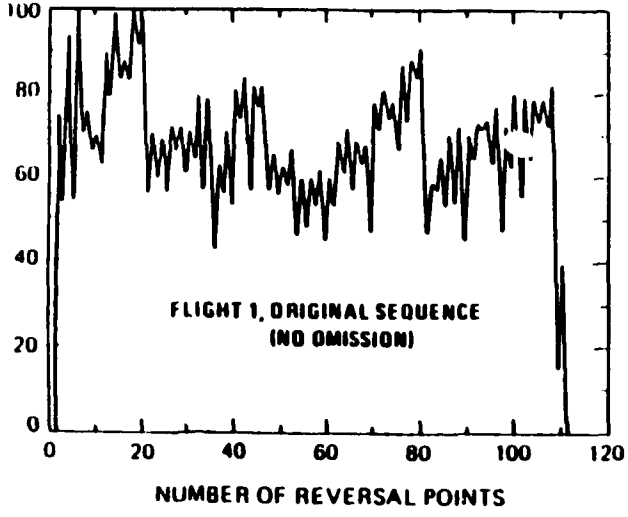

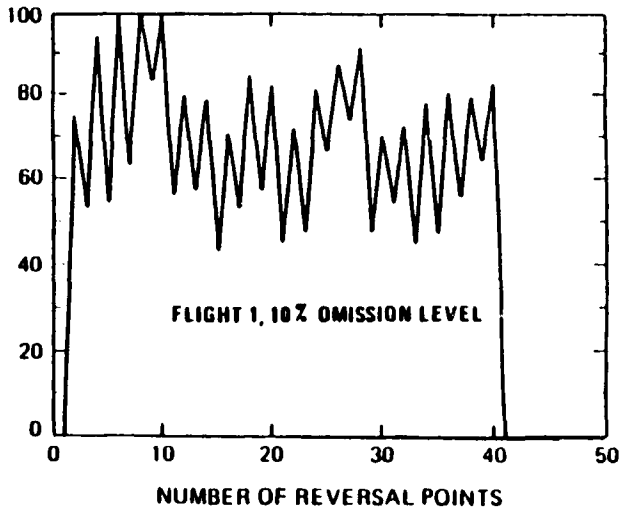

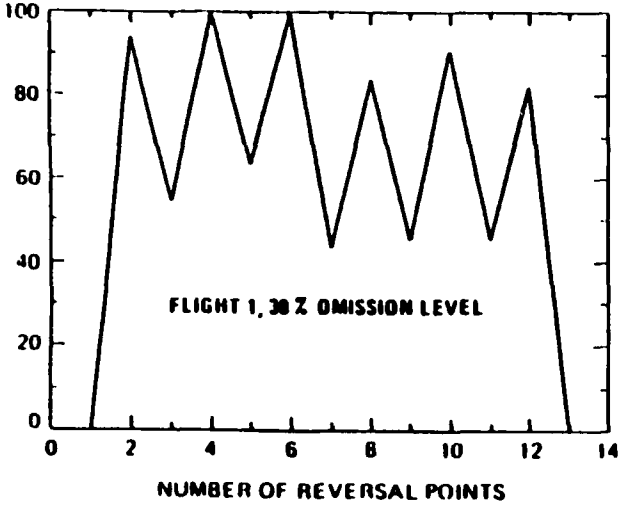

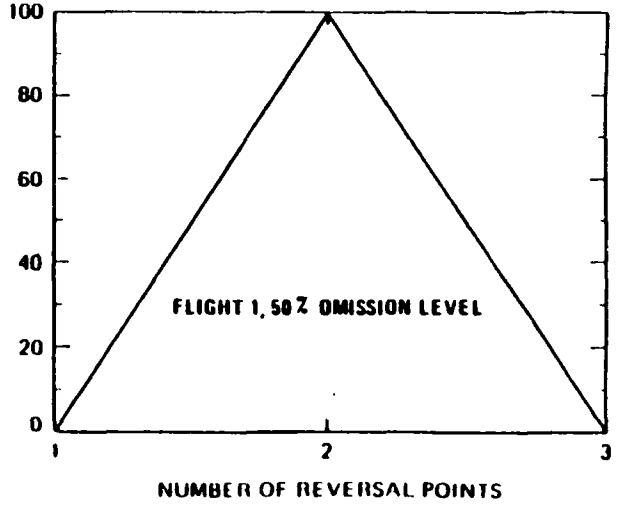

Figure 4. TURBISTAN load history and variations of TURBISTAN used in the NATO/AGARD SUPPLEMENTAL engine disk program.

obtained automatically during peak load excursions using an HP 3456 Digital Voltmeter with 100 nV resolution, while a 10A current was applied through the sample using an HP Programmable Power Supply. The HP 216 computer was used to control all instruments, record EPD measurements, and analyze the final test record.

Tests were generally terminated before complete fracture and the specimens heat-tinted in order to obtain an accurate measure of through-thickness crack length. This value of crack length and corresponding EPD voltage were then used as a single reference point for the calibration expression relating the record of EPD measurements to crack length. The calibration expression used was the same as that used in the original CORE program, developed by Hicks and Pickard [6], and furnished in the following:

$$a/W = B_0 + B_1(V/V_o) + B_2(V/V_o)^2 + B_3(V/V_o)^3$$

where:

a is the crack length (as defined in E647),
W is the specimen width,
V is the measured EPD voltage,
V_o is the reference voltage for a/w = 0.241,
B_0 = -0.5051
B_1 = 0.8857
B_2 = -0.1398
B_3 = 0.0002398

The test record of crack length versus cycles was converted to the final form of crack growth rate versus stress intensity range using a seven-point incremental polynominal method, as described in the ASTM Standard E647, "Measurement of Fatigue Crack Growth Rates".[7] For the simplified spectra (Types 1 through 4), crack growth rates were plotted as a function of alternating stress intensity, ΔK. Since in Types 1 through 3 the minimum load is essentially zero, ΔK equals K_{max}. For the Type 4 load spectrum ΔK was based on the minimum and maximum CA loads, not the periodic overload value. For all the TURBISTAN data, growth rates

(m/flight) were plotted against the maximum value of stress intensity which occurs at least once per flight.

Fracture surfaces of failed samples were observed optically and by scanning electron microscopy. Failed samples were examined at a magnification of 3.5X to determine if any plane stress effects were present, as witnessed by the presence of shear lips on the sides of the crack surfaces. Photomicrographs were taken at 500X using an SEM to characterize the fracture surface morphology at various locations along the fracture surface, while fatigue striation spacing was measured at known levels of applied stress intensity to correlate fracture surface data with EPD-determined crack growth data. Striation spacing was measured on samples tested under the simplified load sequences only. Measurements were taken at a minimum of three levels of stress intensity range, based on the average of measurements taken at three positions the width (B) of the fracture surface: approximately 1/4B, 1/2B, and 3/4B. Results of striation spacing measurements were plotted against stress intensity range to show striation-EPD correlation.

SEM examination of fracture surface morphology to characterize crack growth mechanisms was performed on a total of six specimens: four samples representing Types 1 through 4 simplified sequences, and two samples representing TURBISTAN and TURB50.

SECTION 4
RESULTS AND DISCUSSION

4.1 SIMPLIFIED SPECTRUM CRACK GROWTH RESULTS

The results for C(T) specimens tested under the Types 1, 2, and 3 simplified load spectra are furnished in Figures 5, 6, and 7, respectively. Tabulated data is further listed in the Appendix. For the growth rate determination, a cycle was defined as one block of 10 low-amplitude subcycles followed by a ramp back to zero load (i.e. 0-100-0 percent relative load), as illustrated in each figure. Data for two specimens tested under the Type 1 spectrum are in agreement over the majority of the range examined, with a slight divergence observed at stress intensity ranges between 25-35 MPa$\sqrt{m}$. Fracture surface appearance for the two samples were likewise similar. Results presented for the Type 2 loading are based on a single sample. A slight shift in data sets is observed for two samples tested under the Type 3 spectrum. Macroscopic fracture appearance for specimen CP25 was rougher than for CP26, with slightly lower growth rates developed for CP25 than for CP26. Such differences between the two data sets might be attributed in part to roughness induced crack closure, whereby the rougher crack surface (CP25) would provide a reduction in the effective stress intensity range and hence crack growth rates. Finally, correlation between visually measured crack lengths and those determined via EPD techniques were generally less than 0.2 mm, with differences believed more a result of errors in the visual surface crack length readings.

In addition to the data points shown in each figure, a best-fit polynominal equation was fitted through the data for each simplified spectrum of the following form:

$$\log (da/dN) = C_0 + C_1 (\log K) + C_2 (\log K)^2 + \ldots$$

These curves are also presented in the composite plot shown in Figure 8, along with reference data for Ti-6-4 forging obtained in the core program under CA, R=0.1 type loading. Results based on the best-fit curves demonstrate the effect of the additional subcycles on crack growth behavior. Fatigue crack growth rates

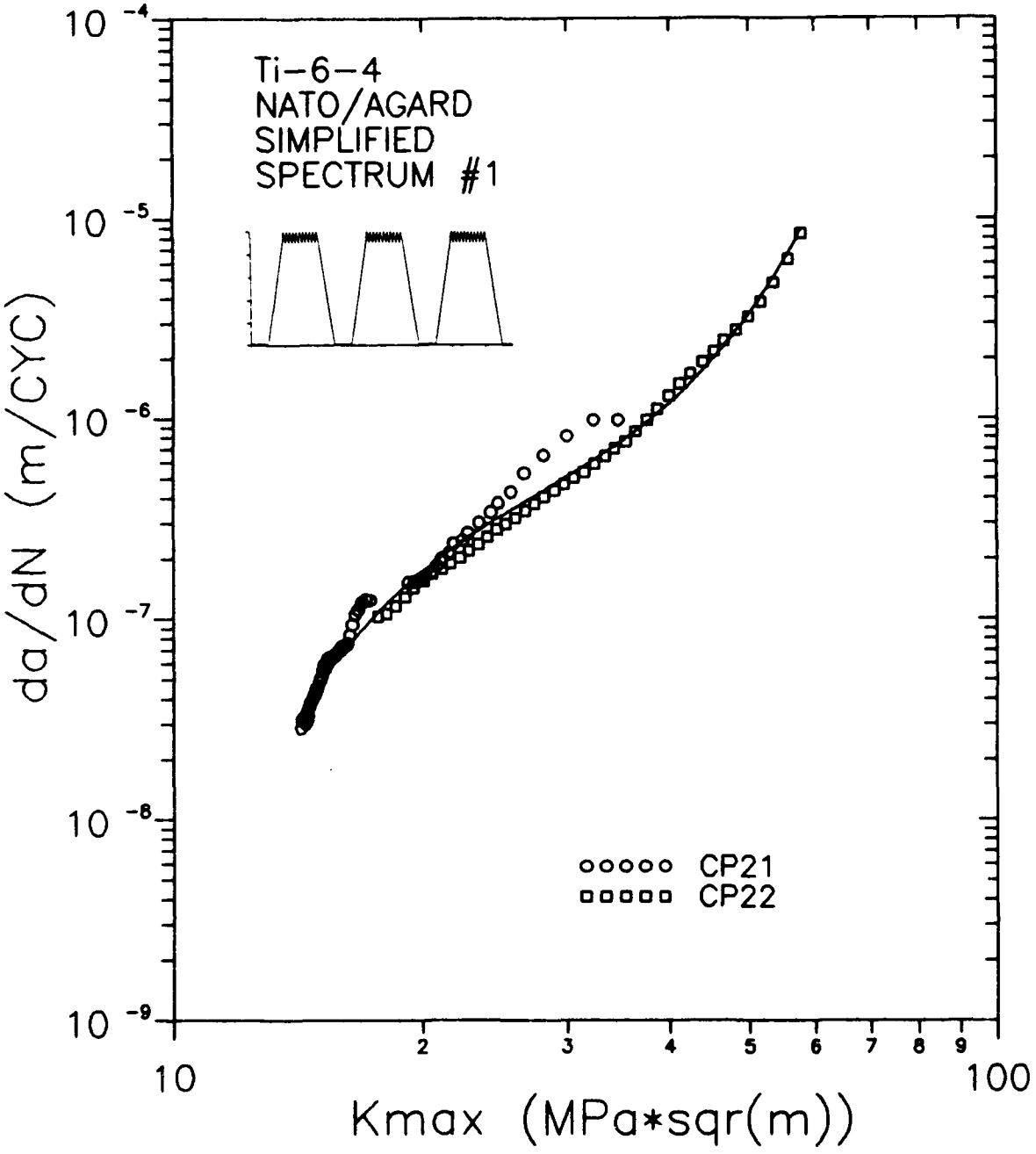

Figure 5. Fatigue crack growth rate data for Type 1 loading.

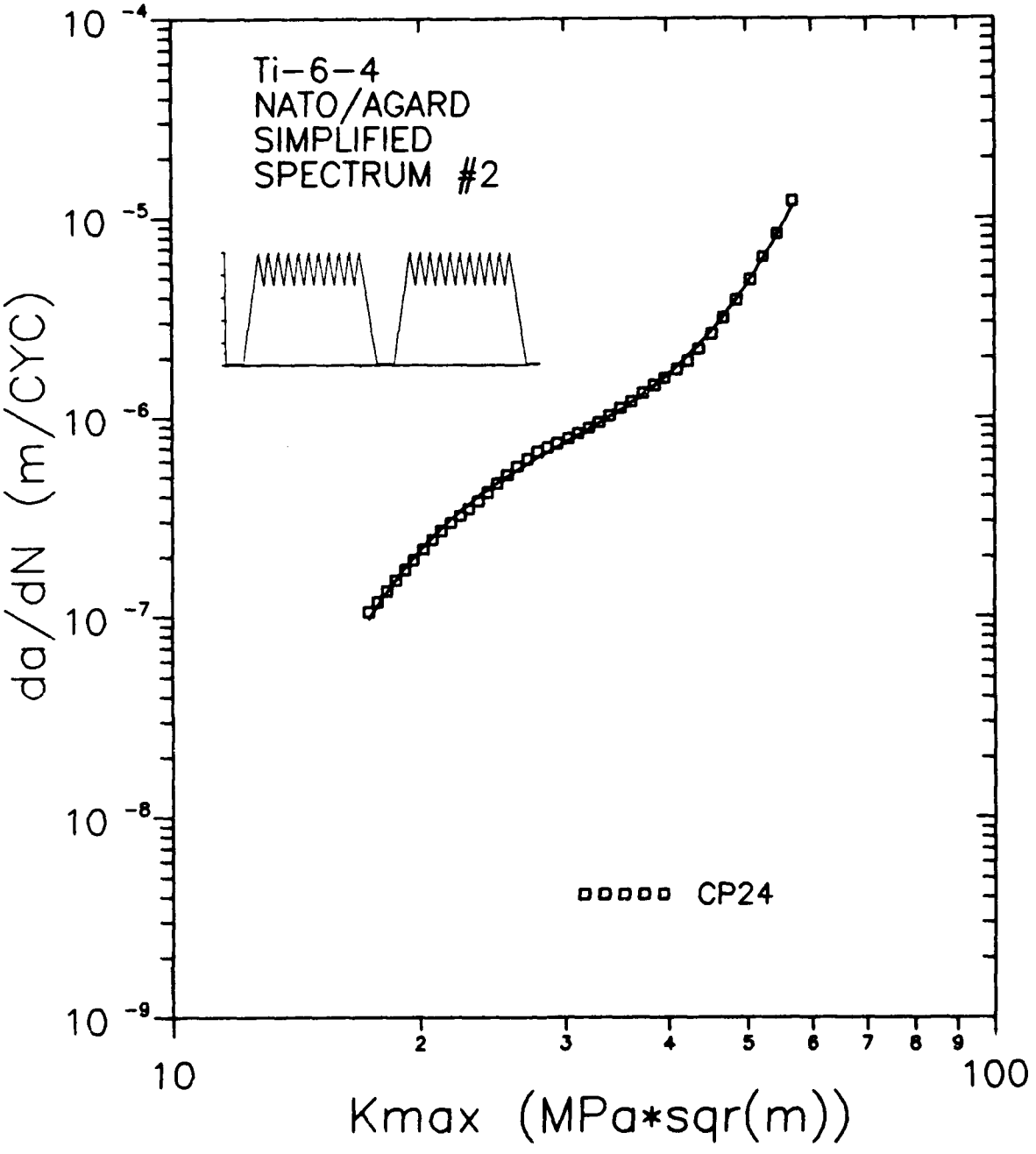

Figure 6. Fatigue crack growth rate data for Type 2 loading.

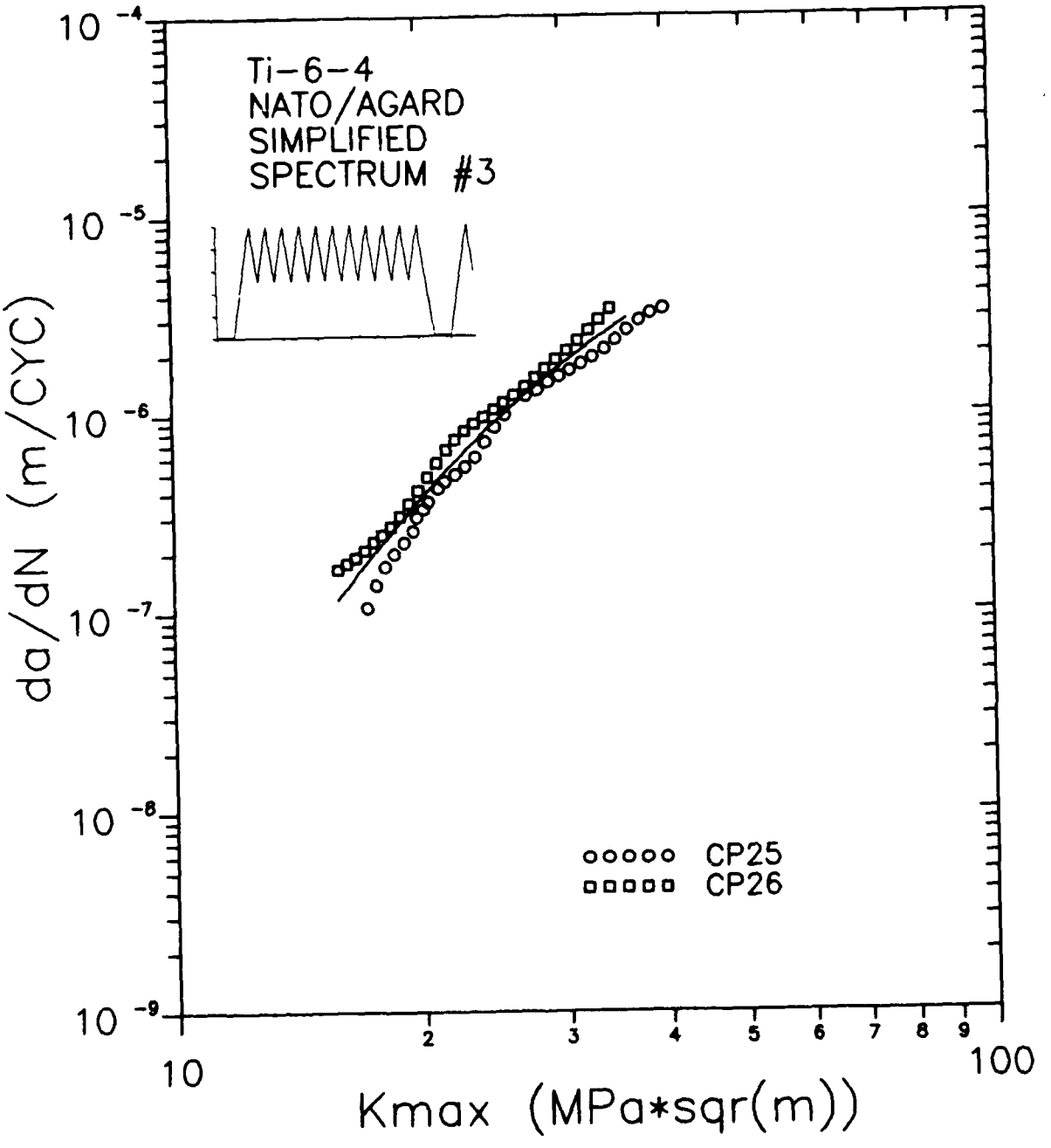

Figure 7. Fatigue crack growth rate data for Type 3 loading.

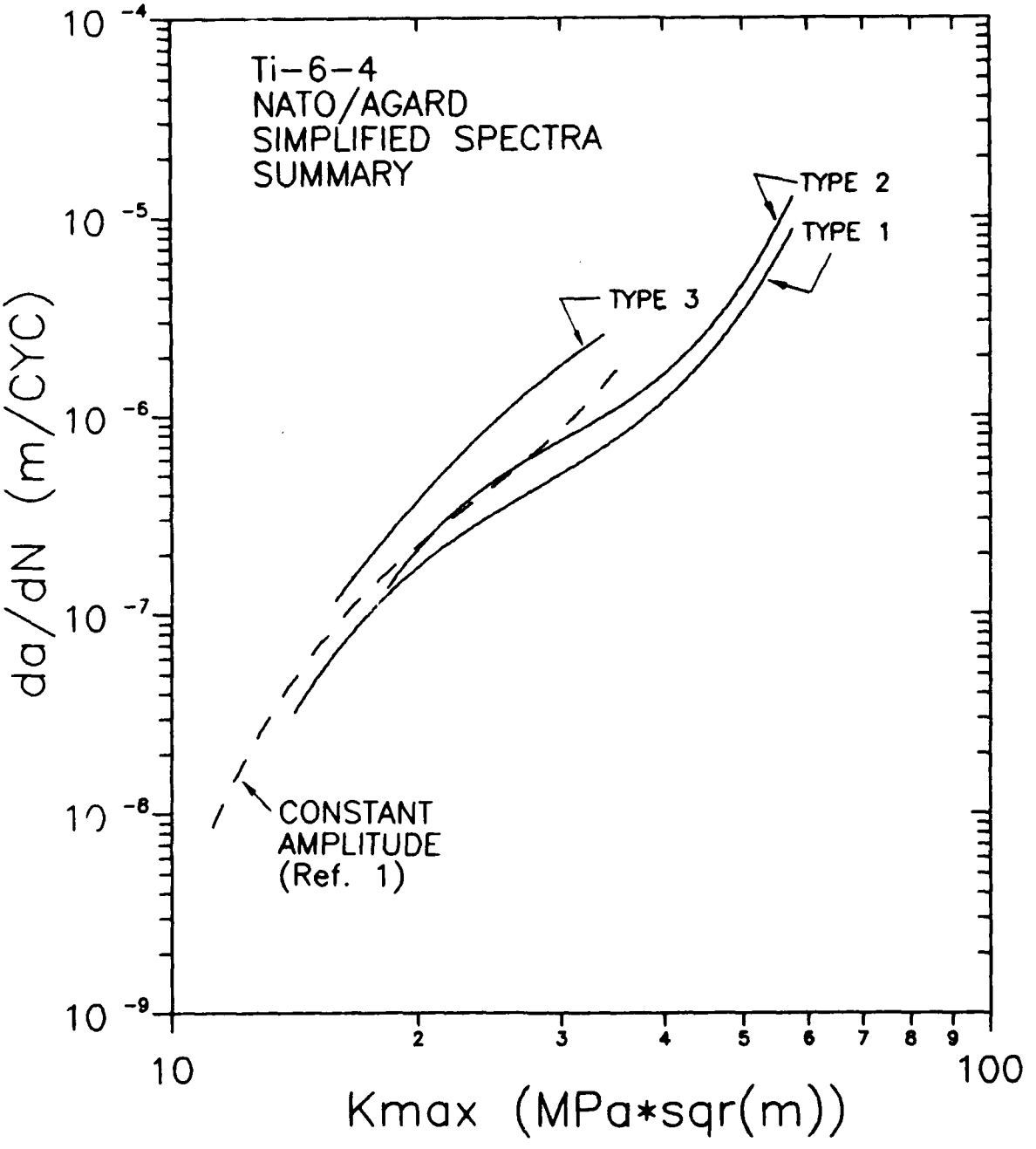

Figure 8. Summary of fatigue crack growth rate data for Types 1 through 3 loading.

increased predictably with increasing spectrum severity, i.e., Type 3 loading which had the highest amplitude subcycles within a major cycle resulted in the highest growth rates. Type 1 loading had the lowest amplitude subcycles and thus produced the lowest growth rates, while the Type 2 load spectrum fell in between the two cases. A lesser difference is observed between the curves representing the Types 1 and 2 load spectra, as compared to the Type 3 results.

The effect of the lower amplitude subcycles becomes more apparent when compared to the CA reference data. Crack growth data for Types 1 and 2 loading are in agreement with the CA data over the limited range available, indicating little effect of the low amplitude subcycles relative to the 0-100-0 percent major load cycle. For the Type 3 loading, an increase in growth rates over the CA data is more evident, with the largest differences occurring at the higher stress intensities. Crack growth rates under Type 3 loading are approximately double that of the CA data for stress intensities greater than 20 MPa$\sqrt{m}$; below that such differences diminish.

The data developed for the Type 4 load spectrum is furnished in Figure 9 in a similar format as the previous spectra. Differences between the two samples tested under this type loading are larger than those observed from the previously described testing. Testing conditions for both samples were similar except for the maximum cyclic load: for sample CP27 the maximum load was 2.5 kN, while for CP28 it was approximately 3.5 kN. Fracture appearances of the two samples tested differ considerably with respect to surface roughness, as shown in Figure 10. As expected, the data for the sample with the greater surface roughness (CP27) fell below the data for the sample with the smoother fracture surface (CP28), again indicating the effect roughness induced closure has on reducing the effective stress intensity range. Additional studies to thoroughly characterize the mechanisms responsible for crack closure as suggested herein are beyond the scope of this investigation.

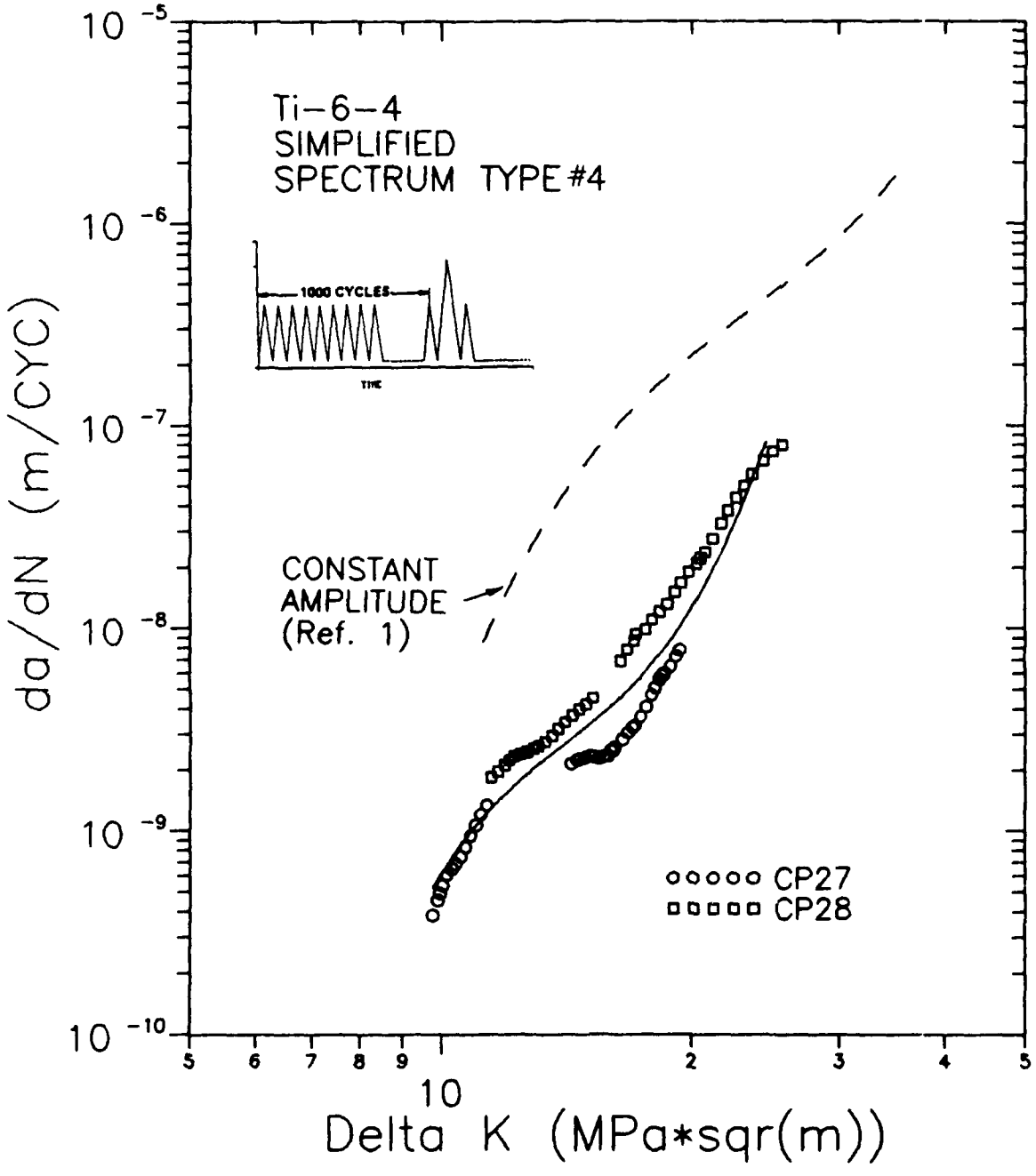

Figure 9. Fatigue crack growth rate data for Type 4 loading.

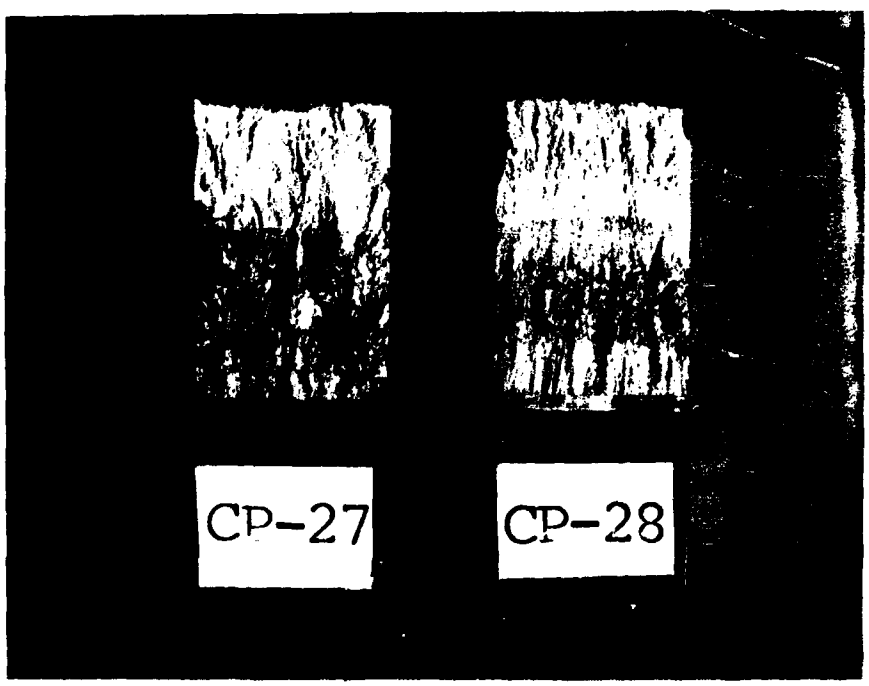

Figure 10. Fracture surface appearance of specimen CP27 and CP28 under Type 4 loading.

For the Type 4 loading case the beneficial effect of the 70 percent overload is clearly evident when comparisons are made with the CA data. A decrease in growth rates of over 10-fold is observed as a result of the periodic overload, which appears consistent over the range of stress intensities examined. Such behavior is attributed to load interaction/retardation effects, where a larger plastic zone is created by the overload cycle which reduces the localized crack driving force and hence growth rates due to an increase in the plasticity-induced crack closure loads.

4.2 SIMPLIFIED SPECTRUM FRACTOGRAPHY

Optical examination of the fracture surfaces showed no evidence of any plane stress effects on the sides of the fatigue crack surfaces for any of the specimens tested under Types 1 through 4 loading. This indicated that plane strain conditions prevailed throughout all testing. In the overload region, produced afer completion of the fatigue testing, shear lips representing less than 5 percent of the total specimen thickness, were observed for all specimens.

Representative views of the fracture surfaces, based on SEM examination, for Types 1 through 3 loading at three stress intensity ranges are shown in Figures 11 through 13. The fracture surfaces all exhibit similar features. At low stress intensity ranges of approximately 18-20 MPa$\sqrt{m}$, transgranular faceting is the dominant mode of crack propagation. These transgranular facets are much smoother for the Type 1 loading than for the Types 2 and 3 loading. Some cleavage facets are also observed on the Types 2 and 3 fracture surfaces. A representative view of these cleavage facets is shown in Figure 14. At these low stress intensity ranges, fatigue striations could not be resolved.

At the higher stress intensity ranges of approximately 30-36 MPa$\sqrt{m}$, each fracture surface exhibits fatigue striations indicating a transgranular mode of crack propagation. For the Type 1 loading, these striations are observed on a small number of flat appearing facets. For the Type 2 loading, they cover almost all of the surface, whereas, for the Type 3 loading, they are rougher and are interspersed with rough transgranular features.

$\Delta K = 19.8\ MPa\sqrt{m}$

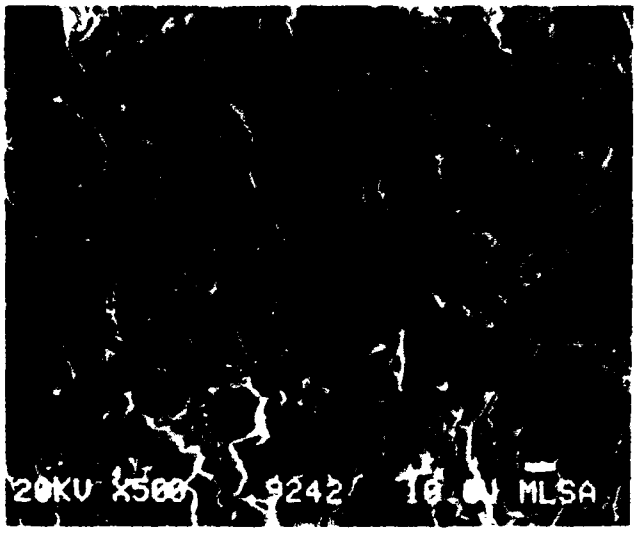

$\Delta K = 27.5\ MPa\sqrt{m}$

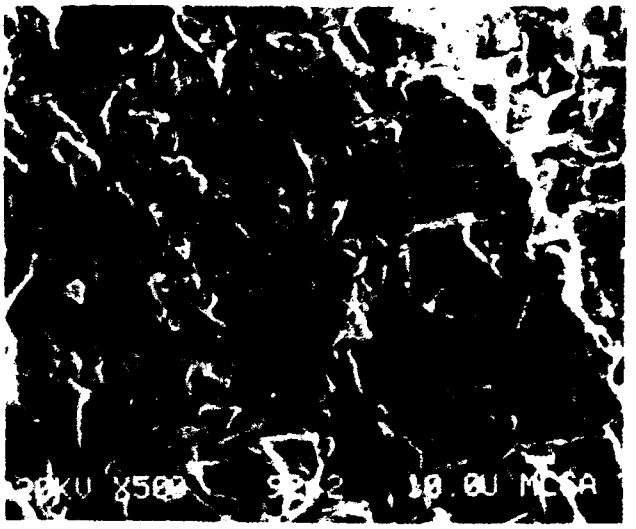

$\Delta K = 36.3\ MPa\sqrt{m}$

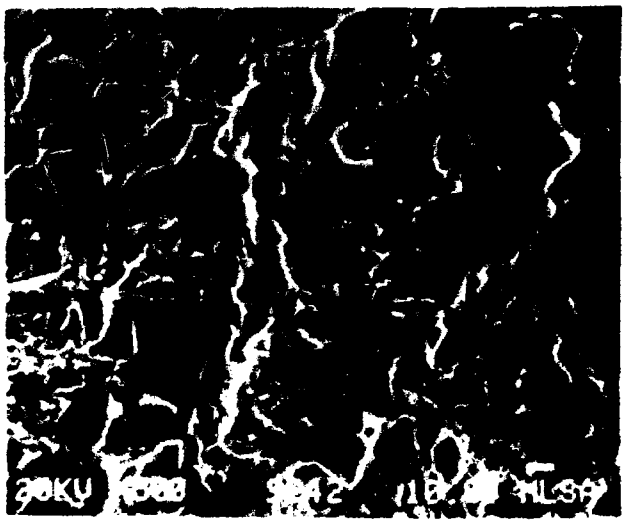

Figure 11. Fracture Surface Morphology for Type 1 Loading (CP22) at 500X. Arrows indicate general direction of crack propagation.

$\Delta K = 17.6\ MPa\sqrt{m}$

$\Delta K = 25.3\ MPa\sqrt{m}$

$\Delta K = 35.2\ MPa\sqrt{m}$

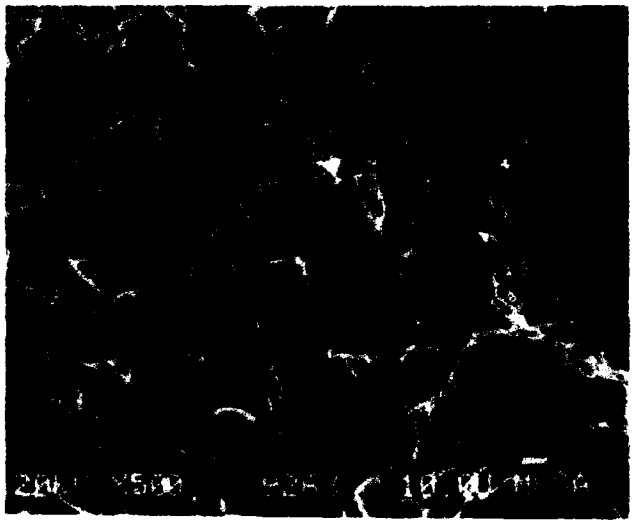

Figure 12. Fracture Surface Morphology for Type 2 Loading (CP24) at 500X. Arrows indicate general direction of crack propagation.

$\Delta K = 17.6$ MPa$\sqrt{m}$

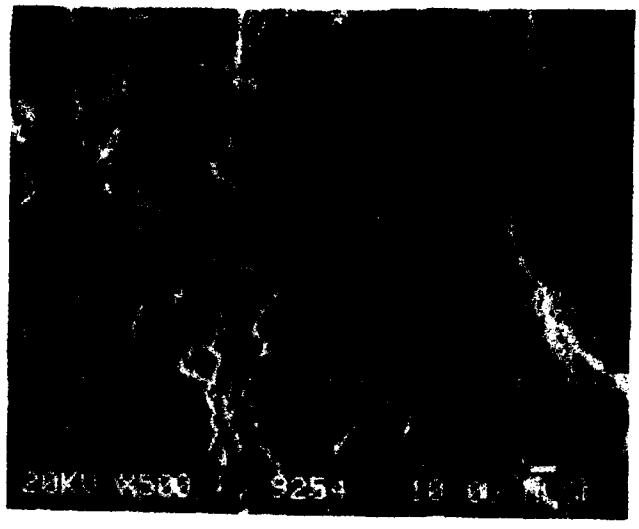

$\Delta K = 26.4$ MPa$\sqrt{m}$

$\Delta K = 30.7$ MPa$\sqrt{m}$

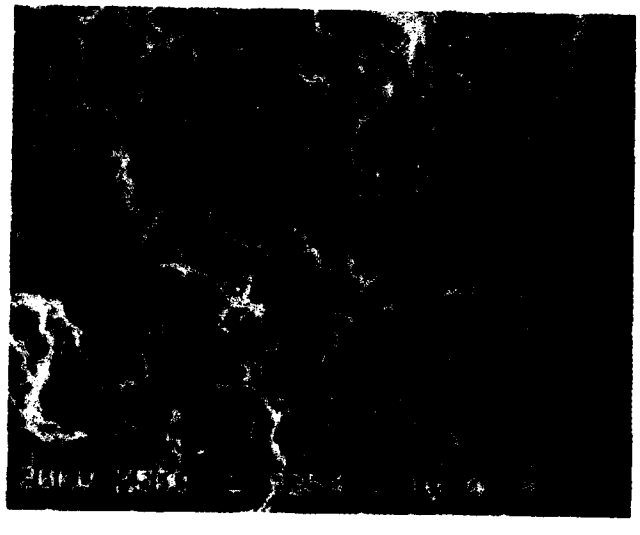

Figure 13. Fracture Surface Morphology for Type 3 Loading (CP26) at 500X. Arrows indicate general direction of crack propagation.

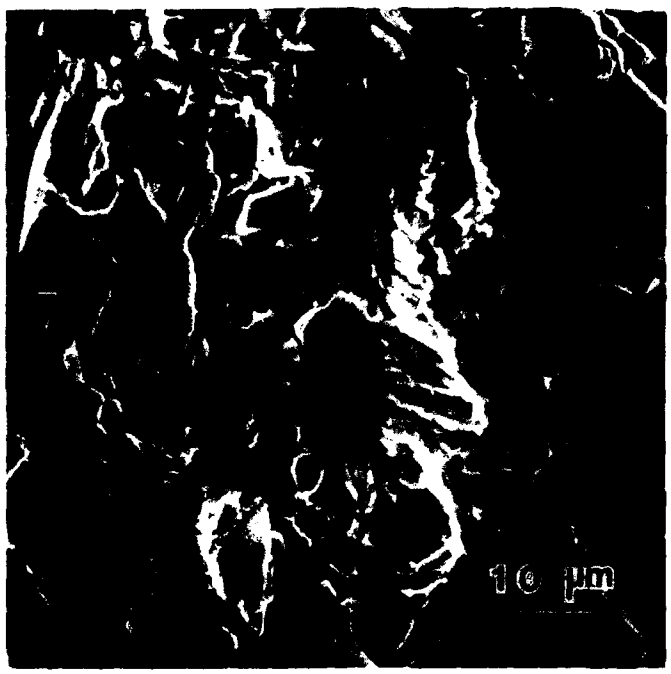

Figure 14. Representative View of Cleavage Facets Found on Types 2 and 3 Fracture Surfaces. Arrow indicates general direction of crack propagation.

Fatigue striation spacing at these high stress intensity ranges supports the crack growth data obtained via the EPD methodology in that the spacing of the Type 1 loading is much smaller than that of the Type 3 loading. As expected, the striation spacing for the Type 2 loading falls in between the two, but is more on the order of the Type 1 loading.

For all stress intensity ranges examined for the Types 1 through 3 loading, secondary cracks were also observed on the fracture surface for each specimen.

Representative views of the fracture surfaces at two levels of stress intensity for the Type 4 loading are shown in Figure 15. At a stress intensity range of 16.5 MPa$\sqrt{m}$, large, blocky appearing striations are the dominant feature on the fracture surface. Smaller striations could not be resolved between these larger striations.

At the higher stress intensity range of 24.2 MPa$\sqrt{m}$, very fine fatigue striations are mixed with rough transgranular features. These striations were barely resolvable at this level of stress intensity. The results of striation spacing measurements for Types 1 through 4 loading are shown in Figure 16. Correlation between EPD determined crack growth data and striation crack growth data is generally 1:1 for the stress intensity ranges where striations were observed. This varies from the CORE program results where differences of 1.7 were reported for the lowest and highest stress intensity ranges.[1] For the Type 4 load sequence, the crack growth rates determined from striation spacings varied considerably from those rates determined from EPD measurements; however, the crack growth rates differed by approximately a factor of 1000. Since the periodic overload for this load sequence occurred every 1000 cycles, the large striations found on the fracture surface appear to be the result of this overload. This factor of 1000 is taken into account for the EPD-striation correlation plot for this load sequence found in Figure 16. At the highest stress intensity range, a divergence is seen between the EPD-striation data, suggesting that a single striation may no longer represent 1000 cycles.

$\Delta K = 16.5\ MPa\sqrt{m}$

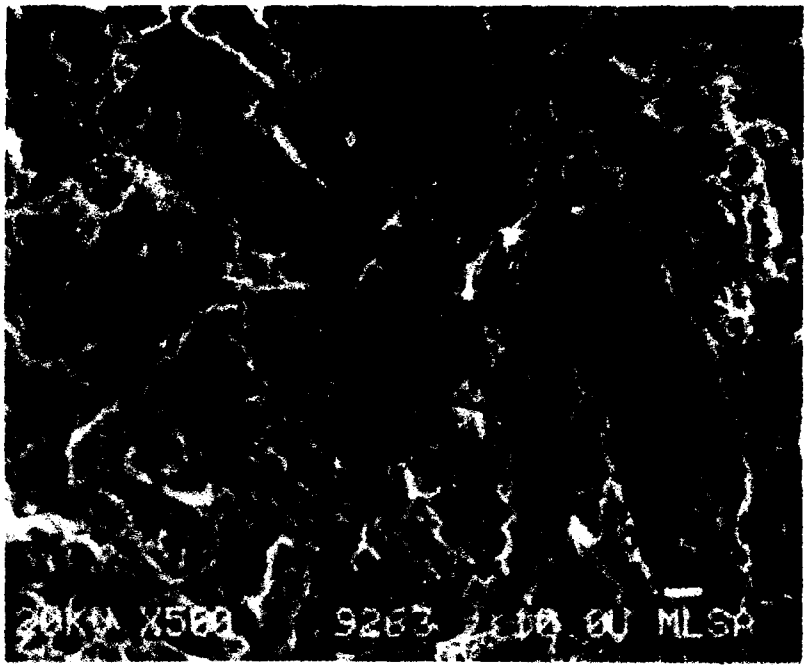

$\Delta K = 24.2\ MPa\sqrt{m}$

Figure 15. Fracture Surface Morphology for Type 4 Loading (CP28) at 500X. Arrows indicate general direction of crack propagation.

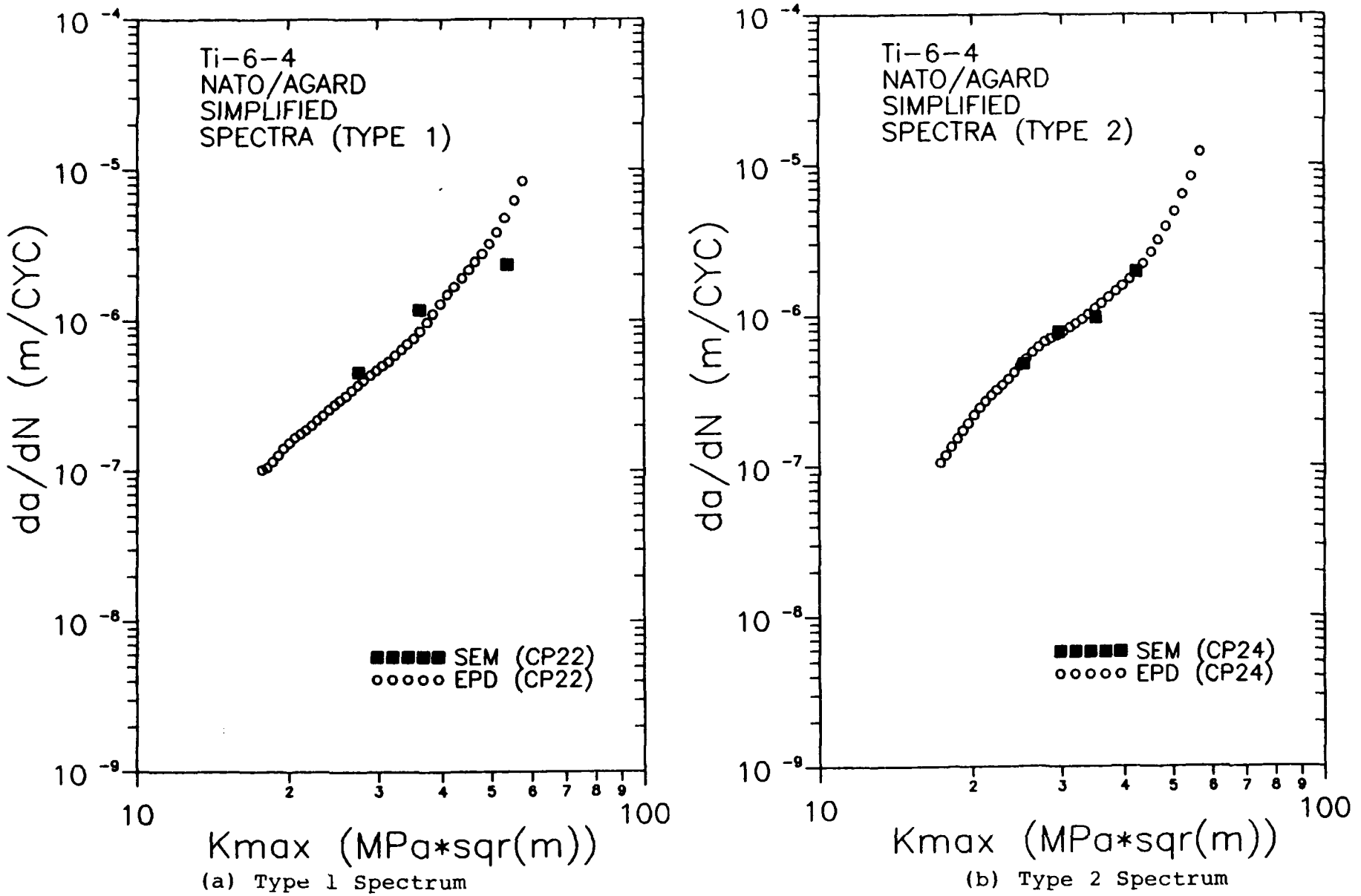

(a) Type 1 Spectrum

(b) Type 2 Spectrum

Figure 16. Comparison of Crack Growth Data Based on Striation Spacing and EPD Measurements for Types 1 Through 4 Loading.

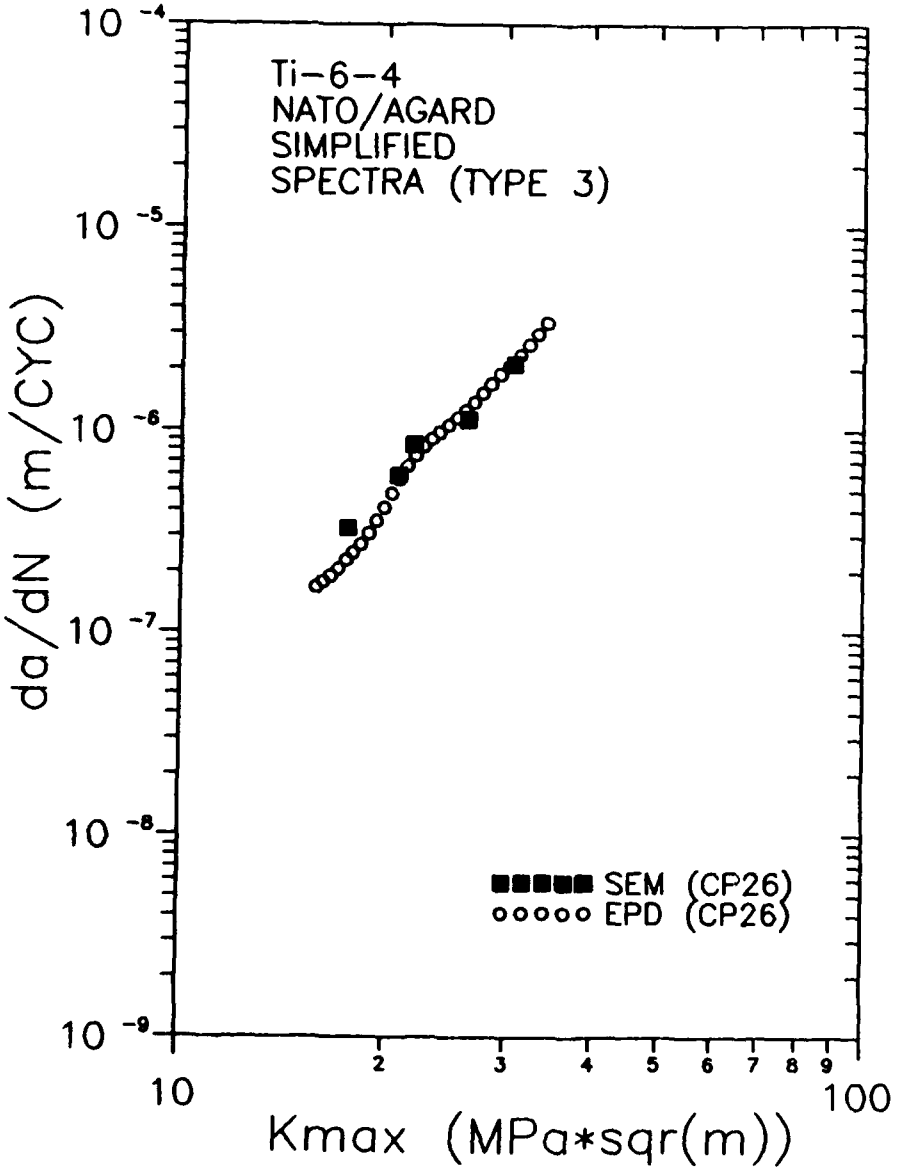

(c) Type 3 Spectrum

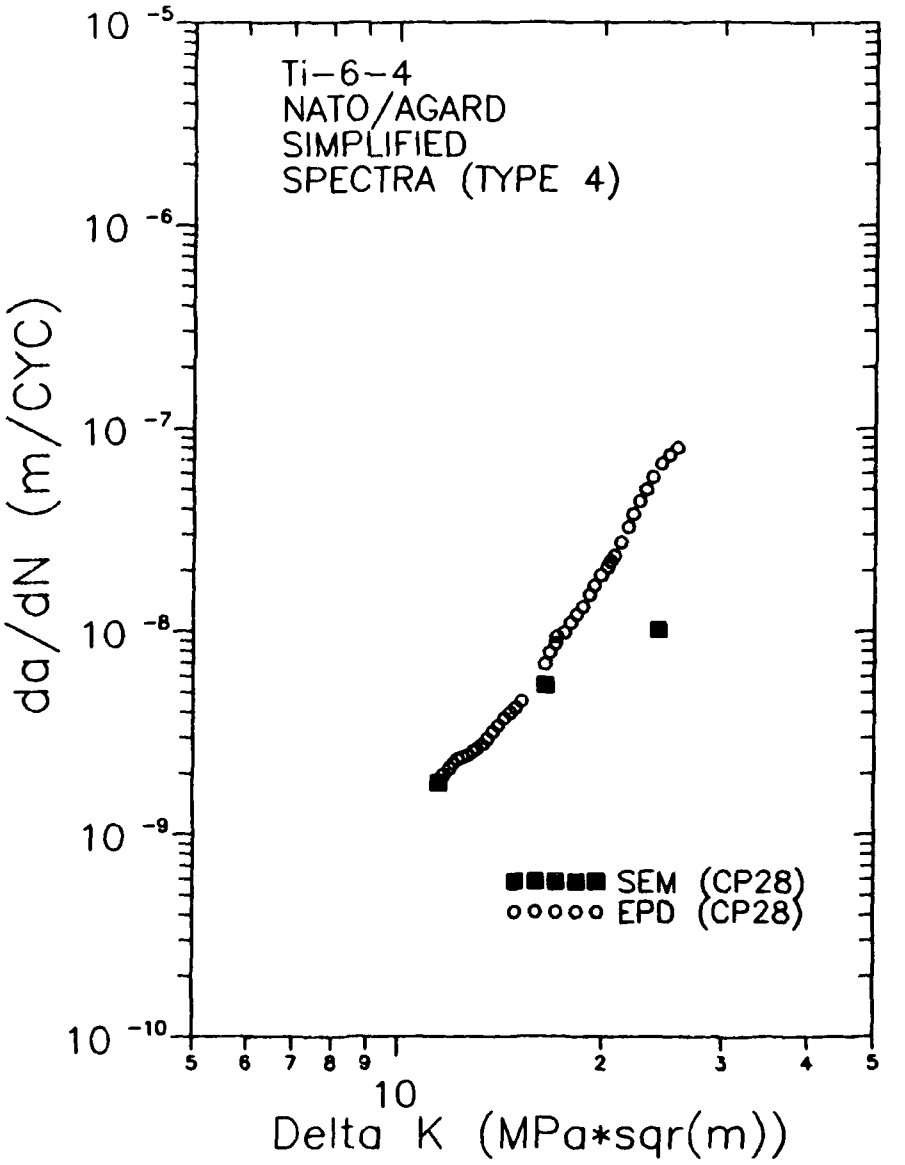

(d) Type 4 Spectrum

Figure 16. Comparison of Crack Growth Data Based on Striation Spacing and EPD Measurements for Types 1 Through 4 Loading (Concluded).

4.3 COMPLEX (TURBISTAN) CRACK GROWTH RESULTS

The results of fatigue crack growth rate testing under the full TURBISTAN spectrum and TURBISTAN with 10, 30, and 50 percent omission levels are presented in Figures 17, 18, 19, and 20, respectively. Crack growth rates per flight are plotted as a function of maximum stress intensity for the interval of flights over which growth rates were determined. Data shown for TURB10 and TURB30 reflect the results of two specimens per condition, while results of a single specimen are furnished for TURB50 and FULL TURB. Since each data set appeared linear (on log-log axes) over the ranges examined, best-fit curves of the form: $da/dF = C*K^n$ were also fitted to each data set and likewise furnished in the respective figures. The data for the two specimens under TURB10 loading are in excellent agreement over the range examined, while a definite shift is observed for the two specimens tested under TURB30. As was in case of the previously described simplified spectra, the fracture surfaces of the two samples tested under TURB30 differed significantly with respect to fracture surface roughness, with the sample with the rougher crack surface (CP30) exhibiting lower crack growth rates than the sample with the smooth fracture surface (CP40). A photo of each is provided in Figure 21. Again, explanations for the differences between growth rate data are based on differences between crack opening loads and hence the effective stress intensity ranges.

The effects of spectrum type on crack growth rates becomes apparent when the best-fit lines from each data set are plotted together, as illustrated in Figure 22. Little or no effect is observed on fatigue crack growth rates when those load excursions 30 percent and below are excluded from the full TURBISTAN spectrum, as witnessed by the near coincident, best-fit lines representing FULL TURB, TURB10, and TURB30. The elimination of those loads excursions up to 50 percent, however, caused a noticeable reduction in growth rates, approximately one-half of those under the other three load spectra. This reduction is consistent throughout the range of stress intensities examined. In light of this, it is apparent that those load excursions in the TURBISTAN load spectrum greater than 30 percent of the peak load contribute

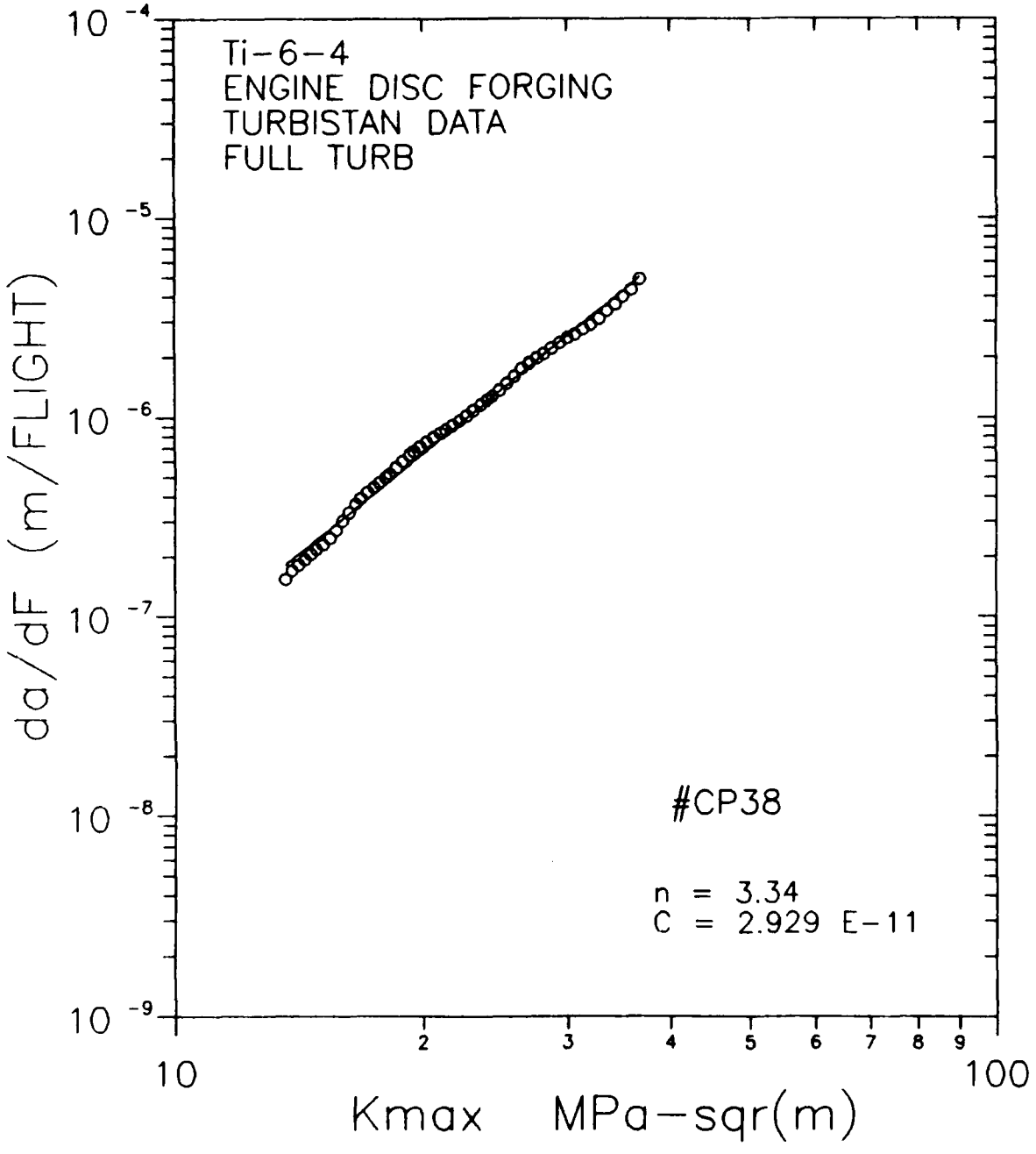

Figure 17. Fatigue crack growth rate data under full TURBISTAN.

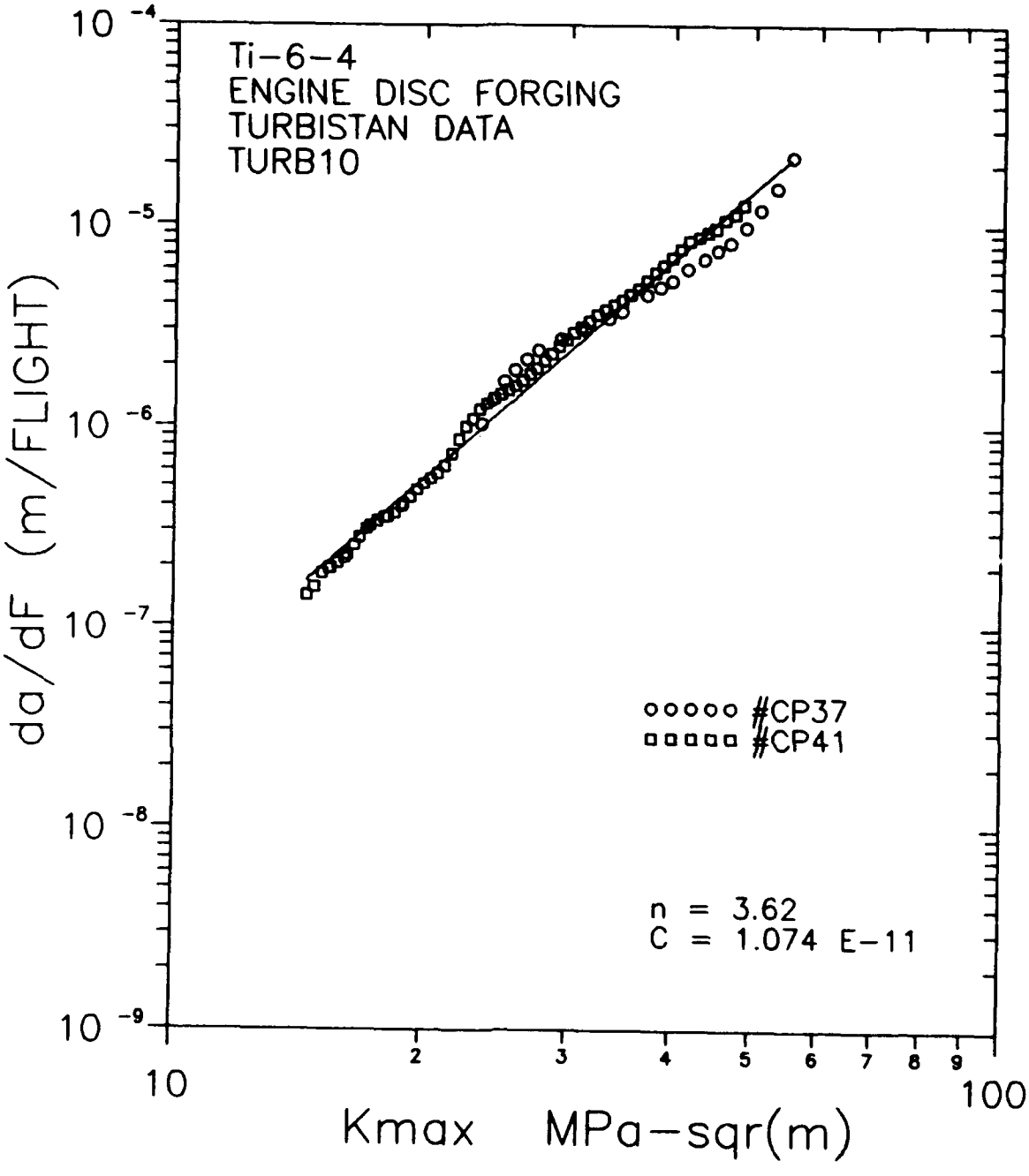

Figure 18. Fatigue crack growth rate data under TURB10.

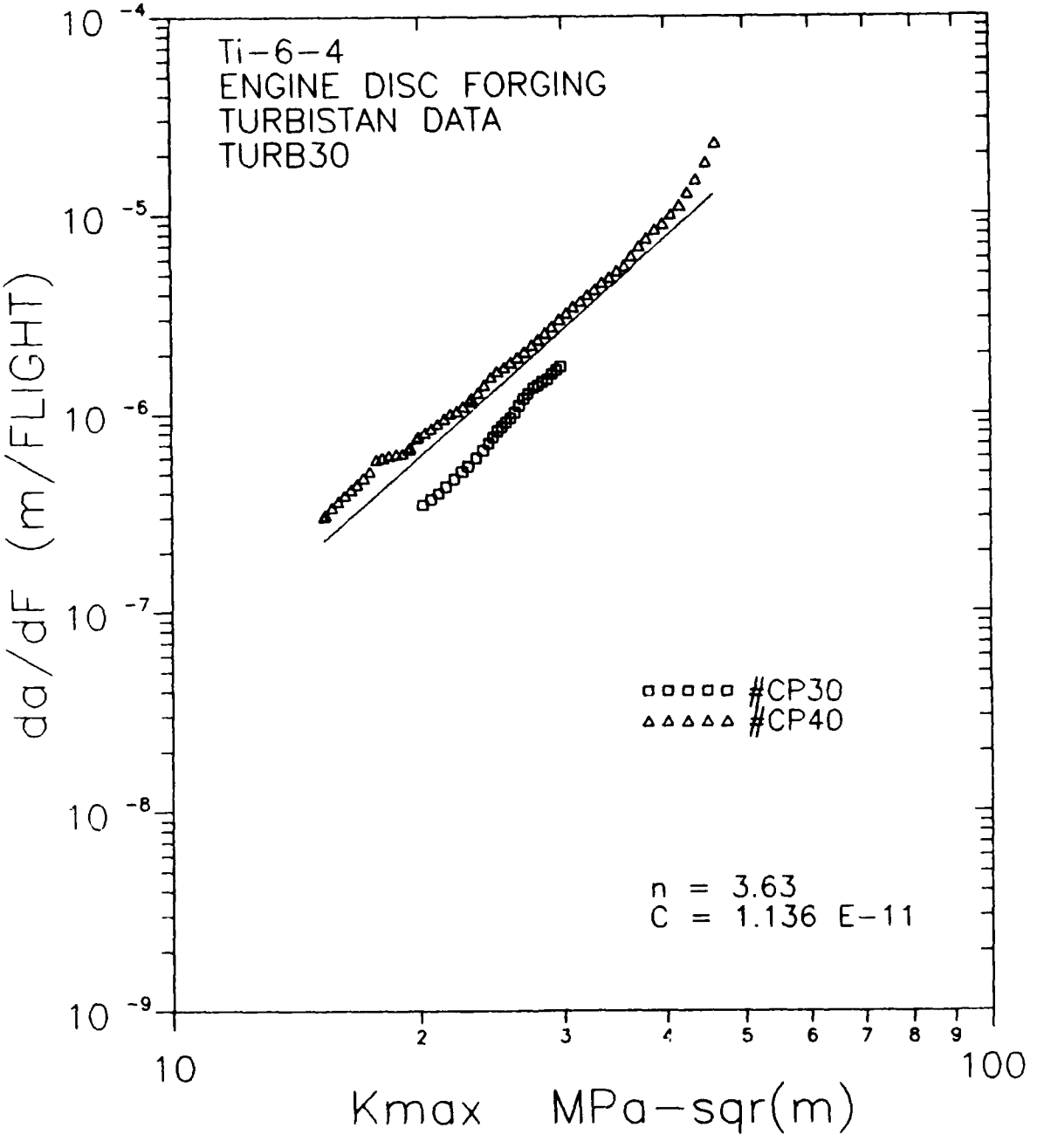

Figure 19. Fatigue crack growth rate data under TURB30.

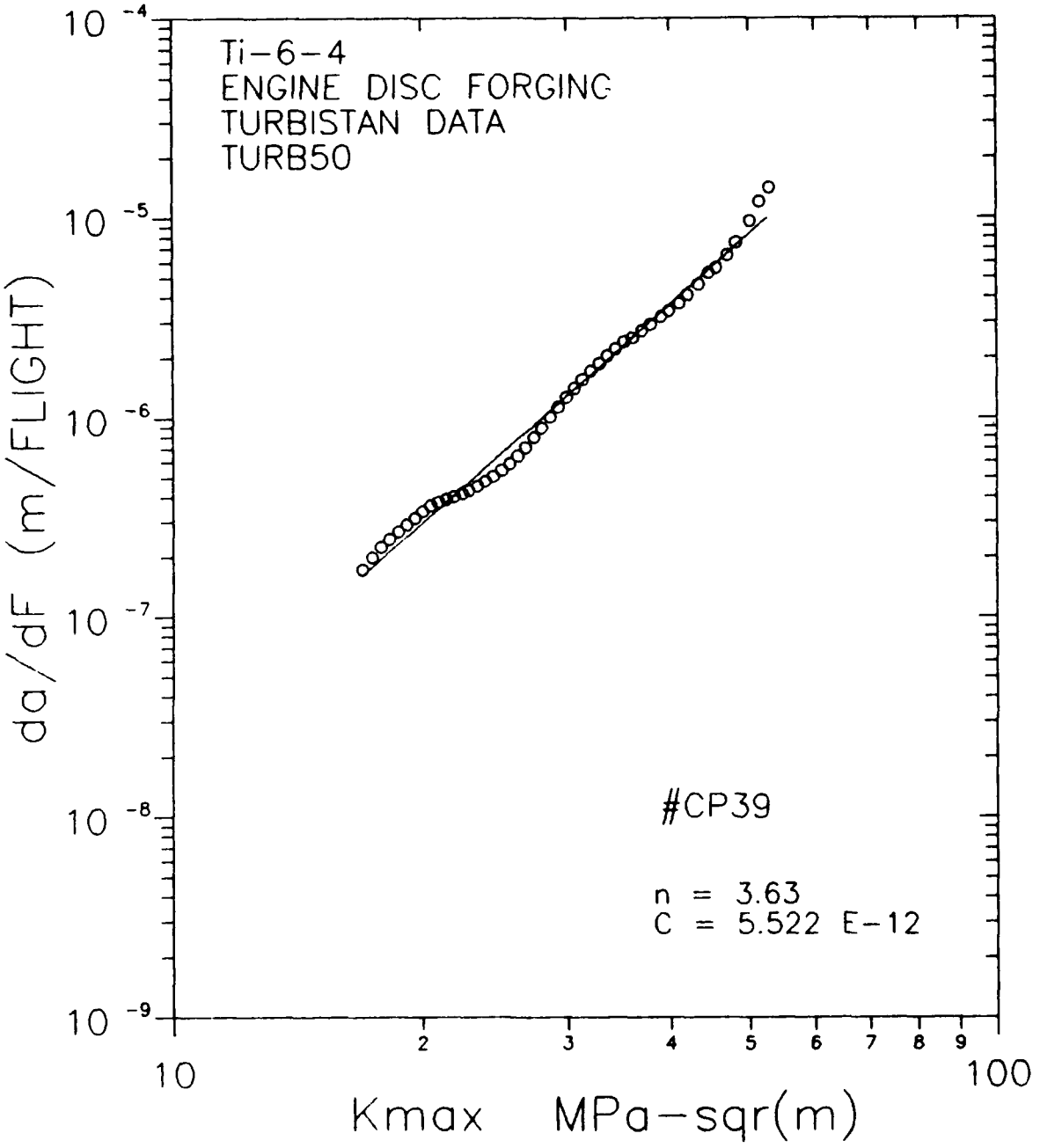

Figure 20. Fatigue crack growth rate data under TURB50.

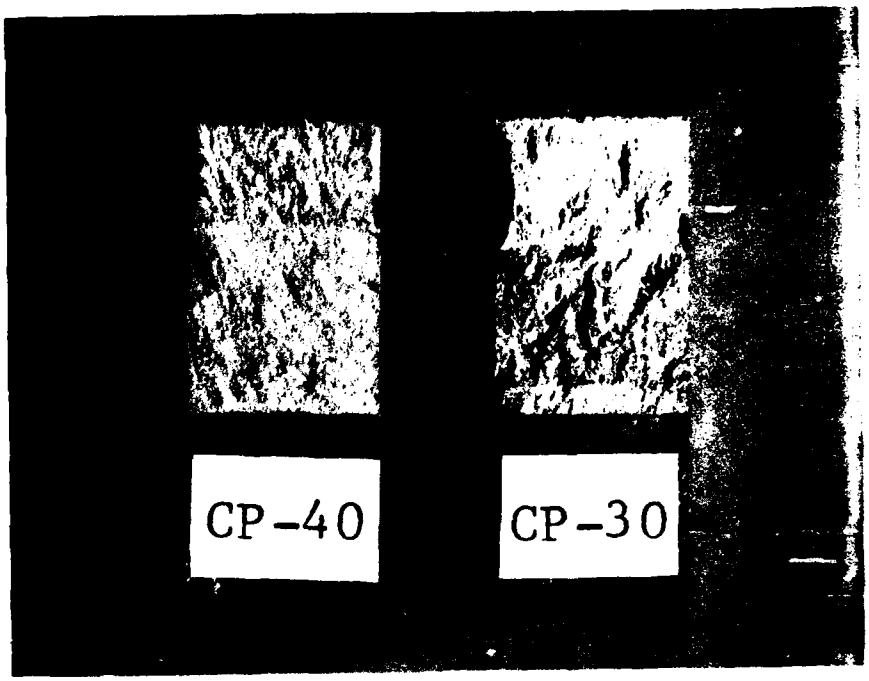

Figure 21. Fracture surface appearance of specimens CP30 and CP40 under TURB30 loading.

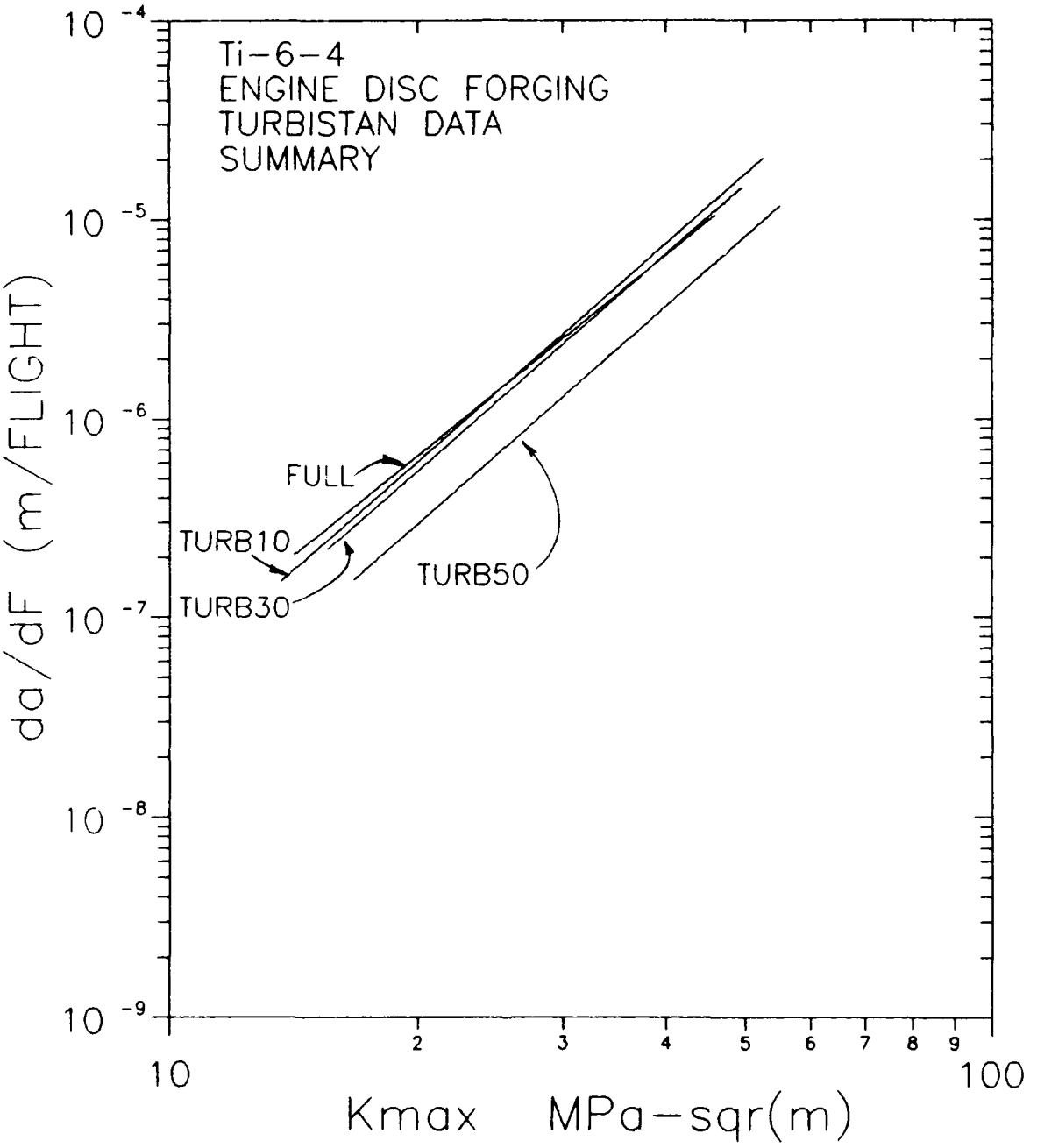

Figure 22. Summary of fatigue crack growth rate data for the various TURBISTAN load sequences.

to fatigue damage, while those excursions below 30% have little influence on crack growth, for the range of stress intensities examined.

4.4 COMPLEX SPECTRUM FRACTOGRAPHY

As with the simplified spectra, optical examination of the fracture surfaces showed no evidence of any plane stress effects on the sides of the crack surfaces for any of the specimens tested under the various TURBISTAN load sequences.

Representative views of the fracture surfaces, based on SEM examination, for TURBISTAN and TURB50 loading at three levels of stress intensity are shown in Figures 23 and 24. At low stress intensity ranges of approximately 18-20 MPa$\sqrt{m}$, both fracture surfaces exhibit transgranular features. The TURB50 surface has a striated appearance and is smoother than the TURBISTAN surface which displays transgranular facets mixed with some cleavage facets.

At the highest stress intensity range of approximately 30-33 MPa$\sqrt{m}$, fatigue striations are observed on both fracture surfaces. These striations, however, are more continuous and cover more of the fracture surface for the TURB50 loading. Secondary cracking was also observed on both surfaces. No striation spacing measurements were made for any of the complex load sequences.

K_{max} = 17.6 MPa$\sqrt{m}$

K_{max} = 23.5 MPa$\sqrt{m}$

K_{max} = 32.8 MPa$\sqrt{m}$

Figure 23. Fracture Surface Morphology for TURBISTAN Loading at 500X. Arrows indicate general direction of crack propagation.

K_{max} = 19.8 MPa$\sqrt{m}$

K_{max} = 28.6 MPa$\sqrt{m}$

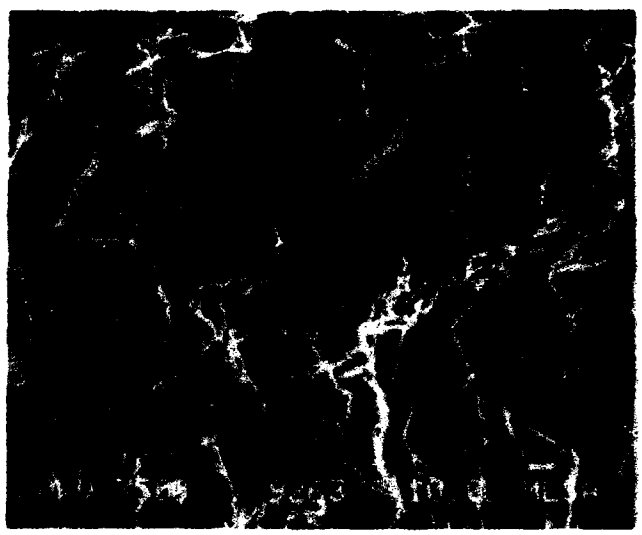

K_{max} = 29.7 MPa$\sqrt{m}$

Figure 24. Fracture Surface Morphology for TURB50 Loading at 500X. Arrows indicate general direction of crack propagation.

SECTION 5
CONCLUSIONS

Based on limited testing of Ti-6-4 disk forging samples under a variety of unique loading conditions, the following conclusions are reached:

1. During constant amplitude loading, the addition of a number of low amplitude subcycles during a "major" load cycle of 0-100-0 percent relative load provided addition fatigue damage only when the amplitude of such subcycles approached 50 percent of the major load cycle. Little or no increase in crack growth rates were observed when subcycles of 10 and 30 percent of the major load cycle were applied.

2. The addition of a 70 percent overload cycle applied once every 1000 constant amplitude cycles proved clearly benificial in regards to fatigue crack growth rates. A 10-fold reduction in crack growth rates was observed when compared to constant amplitude data obtained in the core test program.

3. The exclusion of load cycles from the standard TURBISTAN engine spectrum of 10 and 30 percent of the maximum load had little effect on crack growth rates. Eliminating those load excursions below 50 percent of the maximum spectrum load caused an approximate 50 percent decrease in crack growth rates.

4. Fatigue crack growth rate data based or striation measurements displayed a near 1:1 correlation with data determined via EPD methods over those ranges where fatigue striations were observed.

5. Fracture modes were transgranular with a variety of features observed on the fracture surfaces. In general, at lower stress intensity ranges, transgranular facets including cleavage facets were the dominant fracture surface features, while, at higher stress intensity ranges, fatigue striations were the dominant features.

REFERENCES

1. Mom, A.J. and Raizenne, M.D., "AGARD Engine Disc Cooperative Test Program - CORE Program Results," National Aerospace Laboratory NRL, The Netherlands, Report # NRL MP 86045U, 1987.

2. Ruschau, J.J., "AGARD Engine Disk Material Cooperative Test Program," University of Dayton Research Institute, Report # UDR-TR-86-08, 1986.

3. Tirpak, J.D., "AGARD Cooperative Test Program on Titanium Alloy Engine Disc Material," WRDC Materials Laboratory, Systems Support Division, Report # AFWAL/MLS 86-10, 1986.

4. Raizenne, M.D., AGARD TX114 Test Procedures for Supplemental Engine Disc Test Programme," National Research Council Canada, Report # LTR-ST-1671, June 1988.

5. Ten Have, A.A., "Cold Turbistan - Final Definition of a Standarized Fatigue Test Loading Sequence for Tactical Aircraft Cold Section Engine Discs," National Aerospace Laboratory NLR, The Netherlands, NLR TR 87054L, March 1987.

6. Hicks, M.A. and Pickard, A.C., "A Comparison of Theoretical and Experimental Methods of Calibrating the Electric Potential Drop Technique for Crack Length Determination," Int. Journal of Fracture No. 20, 1982, pp. 91-101.

7. ASTM E647-88a, "Measurement of Fatigue Crack Growth Rates," 1989 Annual Book of ASTM Standards, Vol. 03.01.

APPENDIX

SPEC I.D.: CP21
DATE: 5/31/88
SPECTRUM: TYPE 1

B (mm) =	13.00	**P max (kN) =**	5.34
W (mm) =	25.96	**P min (kN) =**	0

a (mm)	N	Del K (MPa-sqr(m))	da/dN (m/CYC)
7.72	0		
7.72	1010		
7.75	1400		
7.75	1550	14.26	2.30E-08
7.77	2410	14.30	3.08E-08
7.80	3380	14.34	2.85E-08
7.82	4120	14.37	2.90E-08
7.85	5130	14.41	3.15E-08
7.87	5840	14.44	3.22E-08
7.90	6850	14.49	3.22E-08
7.95	7860	14.54	3.42E-08
7.98	8870	14.59	3.41E-08
8.00	9880	14.64	3.59E-08
8.05	10890	14.69	3.50E-08
8.08	11900	14.75	3.77E-08
8.13	12910	14.80	4.04E-08
8.15	13920	14.86	4.22E-08
8.20	14930	14.92	4.58E-08
8.25	15940	15.00	4.76E-08
8.31	16950	15.08	5.03E-08
8.36	17960	15.15	5.31E-08
8.41	18970	15.23	5.52E-08
8.46	19980	15.32	5.96E-08
8.51	20540	15.37	6.00E-08
8.56	21550	15.46	6.34E-08
8.64	22560	15.57	6.33E-08
8.69	23570	15.66	6.35E-08
8.74	24140	15.72	6.44E-08
8.79	25150	15.82	6.53E-08
8.86	26160	15.92	6.91E-08
8.89	26630	15.98	7.06E-08
8.97	27640	16.10	7.37E-08
9.04	28640	16.22	7.32E-08
9.12	29450	16.31	7.59E-08
9.17	30460	16.43	8.40E-08
9.25	31470	16.56	9.40E-08
9.35	32480	16.72	1.05E-07
9.45	33070	16.84	1.13E-07
9.55	34080	17.05	1.22E-07
9.68	35090	17.27	1.24E-07
9.80	36100		

9.93	37110		
10.06	38120		
	***** TEST	INTERRUPTION	*****
10.72	41240		
10.87	42250		
11.02	43260		
11.18	44270	20.13	1.59E−07
11.48	46060	20.77	1.69E−07
11.58	46800	21.04	1.84E−07
11.79	47810	21.48	2.00E−07
11.89	48430	21.76	2.12E−07
12.14	49440	22.32	2.38E−07
12.27	50020	22.71	2.45E−07
12.55	51030	23.36	2.68E−07
12.83	52040	24.09	3.02E−07
13.00	52880	24.85	3.37E−07
13.31	53590	25.57	3.72E−07
13.61	54310	26.44	4.26E−07
14.02	55320	28.05	5.27E−07
14.50	56230	29.92	6.48E−07
15.04	56990	32.14	8.15E−07
15.52	57570	34.49	9.85E−07
16.23	58310		
16.97	58830		
17.27	58980		

SPEC I.D.: CP22
DATE: 6/15/88
SPECTRUM: TYPE 1

B (mm) =	13.00	P max (kN) =	5.34
W (mm) =	25.96	P min (kN) =	0

a (mm)	N	Del K (MPa-sqt(m))	da/dN (m/CYC)
9.32	0		
9.40	200		
9.65	2640		
9.91	5360	17.65	1.03E-07
10.13	7930	18.11	1.06E-07
10.39	10230	18.56	1.16E-07
10.64	12220	19.02	1.28E-07
10.87	14100	19.51	1.42E-07
11.13	15750	20.01	1.54E-07
11.35	17250	20.53	1.67E-07
11.61	18620	21.06	1.77E-07
11.84	19920	21.60	1.88E-07
12.07	21090	22.15	2.01E-07
12.29	22280	22.75	2.18E-07
12.52	23280	23.34	2.34E-07
12.75	24230	23.95	2.55E-07
12.98	25070	24.59	2.77E-07
13.18	25840	25.24	2.96E-07
13.41	26570	25.92	3.16E-07
13.64	27250	26.63	3.45E-07
13.84	27870	27.38	3.74E-07
14.05	28420	28.13	4.03E-07
14.27	28910	28.90	4.33E-07
14.48	29390	29.74	4.66E-07
14.68	29820	30.59	5.01E-07
14.88	30220	31.46	5.34E-07
15.09	30590	32.38	5.88E-07
15.29	30920	33.33	6.41E-07
15.47	31220	34.29	7.01E-07
15.67	31470	35.26	7.61E-07
15.85	31710	36.27	8.52E-07
16.05	31950	37.47	9.72E-07
16.23	32140	38.63	1.11E-06
16.43	32300	39.81	1.29E-06
16.61	32440	41.06	1.49E-06
16.79	32560	42.40	1.67E-06
16.99	32670	43.82	1.90E-06
17.17	32760	45.24	2.16E-06
17.32	32840	46.63	2.44E-06
17.50	32910	48.16	2.76E-06
17.68	32970	49.73	3.22E-06

17.86	33020	51.54	3.83E-06
18.03	33070	53.59	4.77E-06
18.24	33110	55.75	6.24E-06
18.42	33140	58.01	8.38E-06
18.62	33170		
18.85	33190		
19.10	33200		

SPEC I.D.: CP24
DATE: 7/7/89
SPECTRUM: TYPE 2

B (mm) =	12.98	P max (kN) =	5.34
W (mm) =	26.04	P min (kN) =	0

a (mm)	N	Del K (MPa-sqt(m))	da/dN (m/CYC)
8.99	0		
9.19	2020		
9.47	5090		
9.73	7800	17.33	1.06E-07
9.98	10180	17.77	1.19E-07
10.24	12310	18.23	1.35E-07
10.49	14130	18.70	1.53E-07
10.74	15690	19.19	1.73E-07
10.97	17020	19.66	1.93E-07
11.23	18280	20.18	2.19E-07
11.48	19380	20.72	2.45E-07
11.71	20330	21.26	2.71E-07
11.96	21180	21.82	2.97E-07
12.19	21940	22.39	3.22E-07
12.42	22630	22.98	3.48E-07
12.65	23280	23.58	3.80E-07
12.88	23880	24.23	4.19E-07
13.11	24420	24.90	4.65E-07
13.33	24880	25.57	5.15E-07
13.56	25320	26.32	5.68E-07
13.79	25700	27.06	6.17E-07
14.02	26060	27.84	6.68E-07
14.22	26360	28.61	7.05E-07
14.43	26640	29.39	7.41E-07
14.66	26930	30.27	7.85E-07
14.86	27200	31.18	8.34E-07
15.06	27440	32.08	8.88E-07
15.27	27660	33.01	9.46E-07
15.47	27870	34.02	1.02E-06
15.67	28060	35.06	1.12E-06
15.88	28250	36.21	1.21E-06
16.08	28410	37.38	1.33E-06
16.28	28550	38.50	1.45E-06
16.46	28680	39.80	1.58E-06
16.66	28800	41.04	1.74E-06
16.84	28900	42.35	1.92E-06
17.02	29000	43.77	2.21E-06
17.22	29080	45.25	2.62E-06
17.40	29160	46.94	3.14E-06
17.60	29220	48.68	3.88E-06
17.81	29270	50.54	4.91E-06

17.98	29310	52.61	6.36E-06
18.19	29340	54.67	8.33E-06
18.39	29360	57.13	1.22E-05
18.62	29380		
18.85	29400		
19.18	29400		

SPEC I.D.: CP25
DATE: 7/20/88
SPECTRUM: TYPE 3

B (mm) =	13.00	P max (kN) =	4.45
W (mm) =	25.98	P min (kN) =	0

a (mm)	N	Del K (MPa-sqr(m))	da/dN (m/CYC)
10.90	8750		
11.13	12640		
11.15	13960		
11.40	16380	17.16	1.07E-07
11.66	18510	17.60	1.40E-07
11.89	20180	18.11	1.73E-07
12.12	21540	18.59	1.98E-07
12.37	22570	19.03	2.25E-07
12.60	23470	19.51	2.57E-07
12.67	24020	19.84	3.03E-07
12.85	24550	20.21	3.37E-07
12.98	24850	20.44	3.64E-07
13.21	25360	20.98	4.25E-07
13.36	25830	21.49	4.59E-07
13.61	26290	22.07	4.99E-07
13.82	26710	22.67	5.46E-07
14.05	27120	23.37	6.11E-07
14.27	27480	24.04	7.25E-07
14.48	27780	24.76	8.61E-07
14.68	28030	25.49	9.88E-07
15.11	28420	27.03	1.23E-06
15.32	28550	27.70	1.31E-06
15.52	28720	28.69	1.44E-06
15.72	28860	29.61	1.56E-06
15.93	28990	30.51	1.68E-06
16.13	29100	31.46	1.83E-06
16.33	29210	32.55	1.96E-06
16.54	29310	33.70	2.15E-06
16.74	29400	34.82	2.37E-06
16.92	29480	36.01	2.62E-06
17.12	29550	37.23	2.96E-06
17.30	29610	38.48	3.23E-06
17.48	29670	39.85	3.40E-06
17.68	29720		
17.86	29770		
17.98	29810		

SPEC I.D.: CP26
DATE: 7/28/88
SPECTRUM: TYPE 3

B (mm) =	13.00	P max (kN) =	4.45
W (mm) =	26.01	P min (kN) =	0

a (mm)	N	Del K (MPa-sqr(m))	da/dN (m/CYC)
9.93	2990		
10.16	4940		
10.41	6600		
10.67	8060	15.83	1.67E-07
10.90	9490	16.25	1.78E-07
11.15	10810	16.67	1.91E-07
11.38	12020	17.08	2.08E-07
11.61	13180	17.53	2.29E-07
11.84	14110	17.94	2.48E-07
12.07	14980	18.38	2.74E-07
12.29	15800	18.87	3.09E-07
12.52	16580	19.39	3.52E-07
12.75	17210	19.91	4.10E-07
12.98	17720	20.40	4.86E-07
13.18	18170	20.97	5.70E-07
13.41	18560	21.55	6.59E-07
13.64	18850	22.09	7.47E-07
13.84	19130	22.71	8.30E-07
14.05	19370	23.33	8.98E-07
14.27	19600	23.98	9.67E-07
14.48	19810	24.66	1.05E-06
14.68	20010	25.37	1.14E-06
14.88	20180	26.07	1.25E-06
15.09	20340	26.84	1.38E-06
15.29	20490	27.66	1.54E-06
15.49	20610	28.47	1.71E-06
15.70	20730	29.39	1.88E-06
15.90	20830	30.28	2.10E-06
16.10	20930	31.27	2.35E-06
16.28	21010	32.25	2.63E-06
16.48	21080	33.25	2.97E-06
16.66	21140	34.28	3.36E-06
16.87	21200		
17.07	21250		
17.27	21290		

SPEC I.D.: CP27
DATE: 9/19/88
SPECTRUM: TYPE 4

B (mm) =	13.00	P max (kN) =	2.50
W (mm) =	26.06	P min (kN) =	0.25

a (mm)	N	Del K (MPa-sqr(m))	da/dN (m/CYC)
12.40	2374260		
12.42	2575960		
12.50	2700580		
12.52	2804090	9.76	3.76E-10
12.65	3084970	9.90	4.54E-10
12.70	3212100	9.96	4.82E-10
12.75	3337920	10.03	5.25E-10
12.88	3547830	10.16	5.96E-10
12.98	3707590	10.28	6.56E-10
13.06	3826310	10.38	6.92E-10
13.18	3991870	10.53	7.53E-10
13.31	4164050	10.70	8.33E-10
13.41	4299180	10.86	9.48E-10
13.54	4414300	11.00	1.06E-09
13.64	4519400	11.15	1.22E-09
13.77	4609490	11.32	1.38E-09
13.82	4655140	11.41	1.48E-09
13.94	4730060	11.58	1.68E-09
14.05	4792270	11.76	1.87E-09
14.96	5192270	13.24	2.36E-09
15.21	5298880	13.74	2.27E-09
15.32	5346030	13.94	2.16E-09
15.39	5380210	14.11	2.11E-09
15.49	5430810	14.32	2.12E-09
15.60	5484110	14.56	2.23E-09
15.65	5506840	14.67	2.25E-09
15.75	5544780	14.87	2.30E-09
15.85	5588070	15.11	2.33E-09
15.90	5611440	15.24	2.31E-09
16.00	5656890	15.48	2.27E-09
16.08	5692420	15.67	2.40E-09
16.15	5723300	15.86	2.50E-09
16.21	5745130	16.00	2.28E-09
16.26	5759040	16.08	2.57E-09
16.28	5772900	16.17	2.55E-09
16.31	5793670	16.31	2.59E-09
16.41	5816050	16.46	2.70E-09
16.48	5851430	16.75	3.15E-09
16.56	5875660	16.98	3.28E-09
16.61	5886270	17.05	3.28E-09
16.71	5914640	17.35	3.68E-09

16.79	5939920	17.62	4.05E-09
16.89	5963290	17.92	4.71E-09
16.94	5974500	18.09	5.20E-09
17.02	5987570	18.31	5.74E-09
17.07	5995730	18.47	5.87E-09
17.09	6001030	18.58	6.09E-09
17.20	6015850	18.87	6.53E-09
17.27	6029310	19.19	7.21E-09
17.32	6036420	19.36	7.85E-09
17.42	6047430		
17.50	6057240		
17.58	6063590		

SPEC I.D.: CP28
DATE: 11/17/88
SPECTRUM: TYPE 4

B (mm) =	13.00	P max (kN) =	3.56
W (mm) =	25.98	P min (kN) =	0.35

a (mm)	N	Del K (MPa-sqr(m))	da/dN (m/CYC)
10.24	194190		
10.36	275830		
10.52	386140		
10.72	490840	11.49	1.88E-09
10.90	576880	11.70	2.00E-09
11.07	664160	11.93	2.10E-09
11.20	725420	12.09	2.22E-09
11.33	784230	12.25	2.32E-09
11.48	851100	12.47	2.38E-09
11.66	914110	12.68	2.42E-09
11.81	974320	12.89	2.51E-09
11.94	1035680	13.10	2.60E-09
12.09	1098150	13.33	2.76E-09
12.27	1153700	13.56	2.95E-09
12.42	1205300	13.81	3.23E-09
12.60	1256800	14.09	3.48E-09
12.75	1305000	14.36	3.68E-09
12.93	1347100	14.64	3.96E-09
13.08	1385030	14.90	4.18E-09
13.23	1423770	15.21	4.50E-09
13.41	1459560	15.50	5.05E-09
13.56	1493140	15.83	5.90E-09
13.72	1520170	16.16	6.98E-09
13.89	1541890	16.48	7.03E-09
14.02	1557410	16.73	7.95E-09
14.17	1573370	17.02	8.72E-09
14.20	1588190	17.31	9.34E-09
14.40	1599450	17.55	9.88E-09
14.55	1615660	17.95	1.10E-08
14.71	1629530	18.39	1.20E-08
14.86	1642390	18.76	1.30E-08
15.01	1653400	19.15	1.48E-08
15.11	1661360	19.48	1.67E-08
15.27	1669720	19.89	1.89E-08
15.42	1677330	20.33	2.13E-08
15.49	1680420	20.54	2.21E-08

15.57	1684170	20.80	2.36E−08
15.72	1690430	21.26	2.75E−08
15.85	1695430	21.73	3.26E−08
15.98	1699130	22.16	3.82E−08
16.13	1702590	22.65	4.43E−08
16.26	1705690	23.18	5.10E−08
16.41	1708390	23.72	5.78E−08
16.59	1711400	24.45	6.64E−08
16.74	1713600	25.11	7.39E−08
16.89	1715500	25.74	7.91E−08
17.04	1717400		
17.20	1719050		
17.30	1720300		

SPEC I.D.: CP38
DATE:
SPECTRUM: FULL TURB

B (mm) = 13.00 P max (kN) = 4.5
W (mm) = 25.98

a (mm)	N	K max (MPa-sqr(m))	da/dF (m/CYC)
8.53	0		
8.71	1870		
8.86	3160		
9.04	4410	13.66	1.52E-07
9.22	5540	13.91	1.69E-07
9.42	6550	14.16	1.82E-07
9.58	7450	14.41	1.92E-07
9.75	8310	14.65	2.08E-07
9.91	9110	14.89	2.20E-07
10.08	9910	15.16	2.32E-07
10.29	10640	15.44	2.48E-07
10.46	11380	15.73	2.71E-07
10.62	12030	16.02	2.96E-07
10.80	12580	16.28	3.27E-07
10.97	13080	16.58	3.64E-07
11.10	13430	16.81	3.97E-07
11.28	13870	17.14	4.25E-07
11.46	14270	17.46	4.49E-07
11.61	14560	17.71	4.74E-07
11.76	14910	18.04	5.07E-07
11.86	15130	18.26	5.22E-07
12.04	15440	18.59	5.59E-07
12.22	15740	18.95	6.08E-07
12.37	16010	19.33	6.42E-07
12.50	16180	19.57	6.74E-07
12.65	16400	19.92	7.10E-07
12.80	16630	20.29	7.61E-07
12.98	16840	20.69	7.98E-07
13.13	17040	21.11	8.37E-07
13.26	17170	21.39	8.63E-07
13.41	17360	21.81	8.95E-07
13.56	17520	22.23	9.60E-07
13.72	17690	22.66	1.02E-06
13.87	17840	23.13	1.09E-06
14.05	17980	23.60	1.16E-06
14.20	18110	24.10	1.22E-06
14.27	18180	24.37	1.27E-06
14.43	18300	24.84	1.34E-06
14.58	18410	25.36	1.49E-06
14.73	18510	25.92	1.64E-06
14.88	18600	26.46	1.77E-06

15.04	18680	27.02	1.81E-06
15.04	18680	27.03	1.85E-06
15.19	18760	27.60	1.93E-06
15.32	18830	28.18	2.02E-06
15.47	18900	28.77	2.19E-06
15.62	18970	29.45	2.37E-06
15.75	19020	30.07	2.51E-06
15.90	19080	30.72	2.58E-06
16.05	19140	31.47	2.75E-06
16.18	19180	32.14	2.89E-06
16.31	19230	32.88	3.06E-06
16.46	19270	33.59	3.42E-06
16.59	19310	34.37	3.73E-06
16.71	19350	35.21	4.07E-06
16.87	19380	35.93	4.35E-06
16.99	19410	36.89	4.91E-06
17.12	19440		
17.25	19460		
17.37	19480		

SPEC I.D.: CP37
DATE: 2/13/89
SPECTRUM: TURB10

B (mm) = 13.00 P max (kN) = 3.59
W (mm) = 26.01

a (mm)	N	K max (MPa-sqr(m))	da/dF (m/CYC)
15.04	91650		
15.24	91940		
15.42	92230		
15.62	92480	23.54	1.03E-06
15.82	92680	24.32	1.36E-06
16.03	92820	25.06	1.65E-06
16.21	92920	25.70	1.89E-06
16.41	93010	26.53	2.14E-06
16.59	93110	27.46	2.36E-06
16.79	93180	28.34	2.56E-06
16.97	93250	29.18	2.72E-06
17.15	93310	30.21	2.92E-06
17.35	93380	31.29	3.08E-06
17.53	93440	32.36	3.27E-06
17.70	93490	33.47	3.45E-06
17.88	93540	34.65	3.69E-06
18.06	93590	35.84	4.10E-06
18.21	93630	37.11	4.48E-06
18.39	93670	38.48	4.89E-06
18.57	93700	39.73	5.28E-06
18.75	93730	41.50	6.05E-06
18.95	93770	43.51	6.70E-06
19.10	93790	45.08	7.51E-06
19.25	93800	46.20	8.29E-06
19.43	93830	48.90	9.89E-06
19.61	93850	50.83	1.20E-05
19.79	93860	53.11	1.53E-05
19.94	93870	56.01	2.19E-05
20.09	93880		
20.24	93880		
20.42	93890		

SPEC I.D.: CP41
DATE: 5/9/89
SPECTRUM: TURB10

B (mm) = 13.00 P max (kN) = 5.34
W (mm) = 26.01

a (mm)	N	K max (MPa-sqr(m))	da/dF (m/CYC)
7.54	0		
7.75	1300		
7.85	2030		
7.92	2800	14.48	1.40E-07
8.13	4420	14.79	1.57E-07
8.36	5700	15.11	1.84E-07
8.56	6700	15.41	1.94E-07
8.59	6790	15.45	1.99E-07
8.79	7810	15.77	2.10E-07
8.99	8850	16.11	2.25E-07
9.07	9130	16.21	2.30E-07
9.27	9990	16.54	2.54E-07
9.40	10480	16.73	2.79E-07
9.58	11160	17.08	3.01E-07
9.70	11530	17.26	3.16E-07
9.91	12060	17.57	3.36E-07
10.08	12680	17.97	3.56E-07
10.19	12920	18.12	3.60E-07
10.36	13410	18.44	3.72E-07
10.57	13930	18.83	3.99E-07
10.62	14060	18.93	4.05E-07
10.80	14520	19.29	4.35E-07
10.97	14900	19.62	4.77E-07
11.15	15280	20.02	5.25E-07
11.33	15610	20.42	5.51E-07
11.53	15920	20.80	5.80E-07
11.71	16230	21.21	6.29E-07
11.86	16520	21.64	7.23E-07
12.04	16770	22.05	8.72E-07
12.22	16970	22.49	1.01E-06
12.40	17110	22.88	1.10E-06
12.57	17250	23.34	1.21E-06
12.73	17400	23.82	1.30E-06
12.90	17530	24.31	1.36E-06
13.06	17630	24.70	1.43E-06
13.23	17750	25.26	1.52E-06
13.39	17860	25.77	1.58E-06
13.56	17960	26.26	1.70E-06
13.72	18050	26.82	1.83E-06
13.87	18140	27.37	1.95E-06
14.05	18220	27.92	2.10E-06

14.20	18290	28.50	2.29E-06
14.35	18360	29.14	2.50E-06
14.50	18420	29.69	2.68E-06
14.66	18470	30.32	2.91E-06
14.81	18520	30.95	3.15E-06
14.96	18570	31.63	3.35E-06
15.11	18620	32.34	3.55E-06
15.29	18660	33.14	3.73E-06
15.42	18700	33.79	3.97E-06
15.57	18740	34.57	4.23E-06
15.72	18770	35.41	4.55E-06
15.88	18800	36.17	4.88E-06
16.03	18830	37.08	5.39E-06
16.18	18860	38.02	5.85E-06
16.31	18880	38.82	6.33E-06
16.46	18910	39.70	6.91E-06
16.59	18920	40.64	7.64E-06
16.74	18940	41.70	8.33E-06
16.89	18960	42.83	8.79E-06
17.02	18970	43.67	9.31E-06
17.15	18990	44.72	9.75E-06
17.30	19000	46.08	1.09E-05
17.45	19020	47.31	1.15E-05
17.58	19030	48.61	1.26E-05
17.70	19040		
17.83	19050		
17.96	19060		

SPEC I.D.: CP30
DATE: 1/10/89
SPECTRUM: TURB30

B (mm) = 13.00 P max (kN) = 3.59
W (mm) = 26.01

a (mm)	N	K max (MPa-sqr(m))	da/dF (m/CYC)
14.07	69760		
14.25	70290		
14.40	70830		
14.58	71320	20.22	3.44E-07
14.73	71790	20.66	3.64E-07
14.88	72200	21.10	3.98E-07
15.04	72570	21.55	4.30E-07
15.19	72940	22.06	4.71E-07
15.37	73270	22.58	5.10E-07
15.47	73480	22.94	5.41E-07
15.62	73760	23.49	6.04E-07
15.75	73970	23.96	6.83E-07
15.85	74120	24.35	7.52E-07
15.95	74230	24.67	7.94E-07
16.03	74330	25.00	8.40E-07
16.10	74420	25.31	8.74E-07
16.18	74520	25.64	9.02E-07
16.26	74590	25.92	9.52E-07
16.33	74670	26.25	1.02E-06
16.41	74750	26.60	1.10E-06
16.48	74820	26.92	1.18E-06
16.56	74880	27.26	1.24E-06
16.64	74940	27.61	1.31E-06
16.71	74990	27.96	1.35E-06
16.79	75050	28.36	1.42E-06
16.87	75100	28.69	1.52E-06
16.94	75160	29.14	1.58E-06
17.02	75200	29.50	1.69E-06
17.09	75240	29.84	1.75E-06
17.15	75280		
17.22	75310		
17.30	75350		

SPEC I.D.: CP40
DATE: 5/3/89
SPECTRUM: TURB30

B (mm) = 13.00 P max (kN) = 5.33
W (mm) = 25.96

a (mm)	N	K max (MPa-sqr(m))	da/dF (m/CYC)
7.92	0		
8.13	760		
8.28	1360		
8.46	2010	15.30	3.00E-07
8.51	2150	15.35	3.09E-07
8.69	2730	15.64	3.41E-07
8.86	3240	15.92	3.69E-07
9.07	3720	16.21	3.92E-07
9.25	4180	16.53	4.18E-07
9.42	4610	16.82	4.43E-07
9.60	5000	17.11	4.72E-07
9.78	5380	17.43	5.13E-07
9.96	5710	17.73	5.90E-07
10.13	6020	18.09	6.03E-07
10.31	6310	18.43	6.25E-07
10.52	6500	18.67	6.36E-07
10.69	6900	19.15	6.38E-07
10.87	7160	19.48	6.67E-07
10.90	7210	19.53	6.71E-07
11.07	7440	19.88	7.44E-07
11.13	7510	19.98	7.57E-07
11.28	7720	20.33	8.05E-07
11.46	7920	20.69	8.48E-07
11.63	8120	21.07	8.96E-07
11.79	8300	21.46	9.60E-07
11.96	8480	21.87	1.01E-06
12.12	8630	22.26	1.03E-06
12.29	8780	22.66	1.09E-06
12.45	8920	23.06	1.17E-06
12.47	8980	23.23	1.21E-06
12.65	9090	23.60	1.27E-06
12.80	9210	24.03	1.42E-06
12.95	9320	24.50	1.56E-06
13.11	9420	24.95	1.65E-06
13.28	9510	25.45	1.75E-06
13.44	9600	25.93	1.84E-06
13.59	9680	26.44	1.94E-06
13.74	9770	26.96	2.06E-06
13.89	9840	27.48	2.23E-06
14.05	9900	28.01	2.34E-06
14.20	9970	28.59	2.52E-06

14.35	10020	29.13	2.72E-06
14.48	10080	29.71	3.00E-06
14.63	10120	30.30	3.21E-06
14.78	10170	30.92	3.48E-06
14.94	10210	31.56	3.69E-06
15.06	10240	32.22	3.96E-06
15.21	10280	32.88	4.14E-06
15.34	10310	33.52	4.53E-06
15.49	10340	34.23	4.80E-06
15.62	10370	35.01	5.27E-06
15.77	10390	35.66	5.61E-06
15.90	10420	36.54	6.28E-06
16.05	10440	37.29	6.97E-06
16.18	10460	38.18	7.44E-06
16.33	10480	39.04	8.27E-06
16.46	10490	39.79	8.80E-06
16.59	10510	40.92	9.82E-06
16.74	10520	41.71	1.09E-05
16.87	10540	42.77	1.28E-05
16.99	10550	43.78	1.48E-05
17.15	10560	44.94	1.82E-05
17.30	10570	46.19	2.31E-05
17.42	10570		
17.58	10580		
17.70	10580		

SPEC I.D.: CP39
DATE: 4/25/89
SPECTRUM: TURB50

B (mm) = 13.00 P max (kN) = 5.33
W (mm) = 26.00

a (mm)	N	K max (MPa-sqr(m))	da/dF (m/CYC)
8.59	5960		
8.92	8560		
9.22	10840		
9.51	12670	16.95	1.73E-07
9.77	14210	17.43	1.99E-07
10.03	15420	17.86	2.25E-07
10.26	16410	18.27	2.47E-07
10.50	17310	18.71	2.69E-07
10.72	18140	19.16	2.91E-07
10.95	18900	19.61	3.15E-07
11.15	19530	20.03	3.40E-07
11.36	20150	20.50	3.63E-07
11.57	20690	20.95	3.79E-07
11.78	21190	21.40	3.92E-07
11.98	21710	21.90	4.04E-07
12.19	22230	22.42	4.18E-07
12.36	22650	22.84	4.35E-07
12.56	23100	23.37	4.57E-07
12.75	23500	23.89	4.83E-07
12.94	23890	24.43	5.11E-07
13.13	24260	25.00	5.47E-07
13.32	24600	25.56	5.87E-07
13.50	24910	26.14	6.43E-07
13.69	25190	26.74	7.14E-07
13.86	25430	27.36	8.01E-07
14.04	25650	27.98	8.94E-07
14.21	25840	28.61	1.01E-06
14.38	26000	29.27	1.13E-06
14.55	26150	29.96	1.27E-06
14.72	26270	30.65	1.41E-06
14.88	26390	31.35	1.56E-06
15.05	26490	32.07	1.72E-06
15.21	26580	32.85	1.88E-06
15.37	26660	33.61	2.05E-06
15.53	26740	34.39	2.22E-06
15.68	26810	35.25	2.41E-06
15.84	26870	36.07	2.51E-06
16.01	26940	37.06	2.74E-06

16.17	26990	37.97	2.93E−06
16.32	27050	39.10	3.20E−06
16.48	27090	39.93	3.43E−06
16.64	27140	41.14	3.73E−06
16.79	27180	42.14	4.11E−06
16.97	27220	43.45	4.64E−06
17.11	27250	44.72	5.29E−06
17.25	27280	45.69	5.62E−06
17.41	27300	47.08	6.48E−06
17.55	27320	48.25	7.48E−06
17.71	27350	50.15	9.61E−06
17.87	27360	51.48	1.04E−05
18.03	27380	52.94	1.20E−05
18.19	27390		
18.33	27400		
18.46	27410		

*U.S.Government Printing Office: 1990—748-056/24241